# Modelling of macrosegregation: applications and future needs

C. Beckermann

Modelling and simulation of macrosegregation has experienced explosive growth since the pioneering studies of Flemings and co-workers in the mid-1960s. This paper presents a review of recent macrosegregation models, with particular emphasis on their application to selected industrially relevant casting processes. The successes and shortfalls of the models in predicting measured macrosegregation patterns are noted. Although it is still early in their development, advanced macrosegregation models that include a detailed consideration of the solidification microstructure are also reviewed. Recent studies involving direct numerical simulation of macrosegregation related phenomena on a microscopic scale are highlighted. Important issues deserving future research attention are identified.     IMR/378

The author is in the Department of Mechanical and Industrial Engineering, 2412 SC, The University of Iowa, Iowa City, IA 52242, USA (becker@engineering.uiowa.edu).

## Introduction

Producers of virtually all types of cast metal continue to struggle with macrosegregation defects. The rejection of single crystal superalloy turbine blades due to the presence of freckles is only one of the more pressing examples. Not surprisingly, modelling of macrosegregation is still a very active research field,[1–3] since the pioneering contributions by Flemings and co-workers beginning in the 1960s.[4–15] Flemings and co-workers discovered the importance of convection within the mushy zones of solidifying alloys, and derived the basic equation describing macrosegregation due to interdendritic flow. Over the years, this research has led to numerous improvements in industrial casting processes, as well as to a better understanding of convection in the mushy zones of the earth's core, solidifying magmas, and sea ice. The phenomena involved in alloy solidification that lead to macrosegregation are so complex that their quantitative prediction for industrially relevant casting processes is only beginning. The purpose of the present work is to review the current state of the art in modelling of macrosegregation, and to provide an outlook of where the field is going. The emphasis in this review is on the *application* of models to quantitatively predict macrosegregation in cast alloys. The basic derivations of the model equations are adequately reviewed elsewhere.[1,2]

Before proceeding, it is useful to recall that the cause of macrosegregation is the long range advection of alloy species due to the relative movement or flow of segregated liquid and solid during solidification. There are numerous causes of fluid flow and solid movement in casting processes:

- flow that feeds the solidification shrinkage and the contractions of the liquid and solid during cooling
- buoyancy induced flows due to thermal and solutal gradients in the liquid; the thermal and solutal buoyancy forces can either aid or oppose each other, depending on the direction of the thermal gradient and whether the rejected solutes cause an increase or a decrease in the density of the liquid
- forced flows due to pouring, motion of gas bubbles, applied magnetic fields, stirring, rotation, vibration, etc.
- movement of free (equiaxed) grains or solid fragments that have heterogeneously nucleated in the melt, separated from a mould wall or free surface, or melted off dendrites; the solid can either float or settle depending on its density relative to the liquid
- deformation of the solid network due to thermal stresses, metallostatic head, shrinkage stresses, or external forces on the solid shell such as those from the rolls in continuous casting of steel.

All efforts to prevent macrosegregation are aimed at controlling fluid flow and solid movement. Examples include adjustments to the alloy composition or thermal gradients to induce a stable density stratification in the liquid; application of nozzles, baffles, porous materials, centrifugal forces, or electromagnetic fields to redistribute the flow; changes in the riser or mould design to influence the cooling and thermal convection patterns; addition of inert particles (as in composites) to change the effective viscosity of the melt; controlled deformation such as soft reduction during continuous casting of steel to squeeze highly enriched liquid away from the centreline of slabs; and modifications to the grain structure (e.g. grain refiners) that change the resistance to flow through the solid network or the prevalence of equiaxed grains.

Macrosegregation models are generally aimed at understanding the basic mechanisms involved, quantitatively predicting the occurrence and severity of macrosegregation, and performing parametric studies for control and improvement of casting processes. Such models are very complex and require large computing resources in their solutions, because they often must consider many aspects of a solidification process simultaneously. Macroscopic phenomena to be considered include heat transfer, solute transport, fluid flow, solid movement, and solid deformation at the scale of the casting. In addition, one must account for phase equilibrium, nucleation, structure formation, segregation, and flow at various microscopic scales. Any factors that affect the flow and the microstructure also influence macrosegregation, and vice versa.
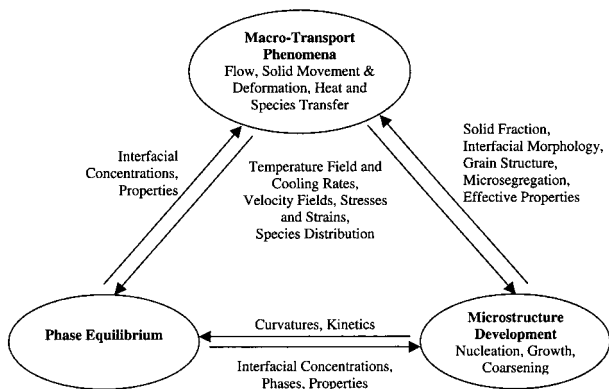
**1 Potentially important interactions in modelling macrosegregation in castings**

Figure 1 illustrates some of these interactions in casting processes. Today, it is certainly not desirable to generate a macrosegregation model that includes all the effects listed in Fig. 1, since a model of such complexity would hardly be useful in practice. Consequently, this review focuses on examples of research where *some* of these interactions are taken into account in order to address industrially relevant macrosegregation problems.

The review is structured as follows. The next section is a brief review of early work (up to the early 1980s) on modelling of macrosegregation. It is simply intended to provide a physical understanding of macrosegregation modelling to a non-specialist reader. The subsequent sections review work in this area that has been performed in the last 10 to 15 years. Six examples are presented of modern macrosegregation models applied to selected casting processes. Following this, a review of macrosegregation models that are coupled to microstructural evolution models is provided. Then, related and increasingly important work on microscale modelling of convection in mushy zones is highlighted. The review concludes by discussing future research needs and directions.

## Basics of macrosegregation modelling

A physical understanding of macrosegregation and its modelling is best obtained by reviewing the pioneering work of Flemings and co-workers in the latter half of the 1960s.[5–7] They considered the flow of interdendritic liquid through a fixed dendritic solid network, as shown in Fig. 2,[4] while accounting for the different densities of the solid and liquid. Flow in the single phase bulk liquid region and movement or deformation of solid were not treated explicitly. In deriving the mass and species balances for the 'mush' volume element in Fig. 2, Flemings and co-workers assumed that: (i) the liquid flowing through it is well mixed and in local equilibrium with the solid (i.e. the liquid is not undercooled) and (ii) there is no solute diffusion in the solid. These are the same assumptions as made in the derivation of the Scheil equation.[26] By combining the equations in a special way, they arrived at the following 'local solute redistribution
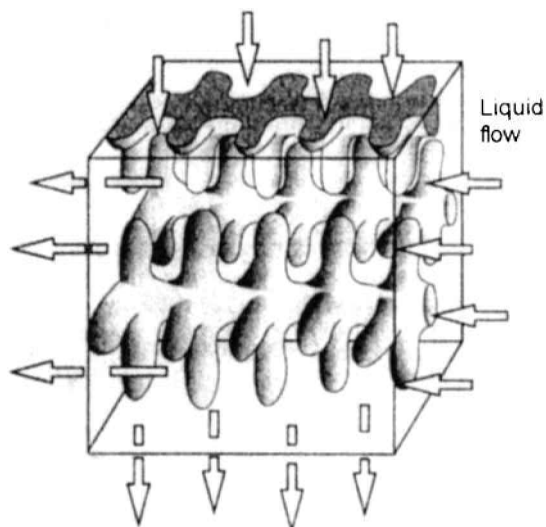


**2 Schematic of liquid flow through fixed dendritic solid skeleton (courtesy M. C. Flemings, MIT)**

equation' (LSRE)[5–7]

$$\frac{\mathrm{d}f_1}{\mathrm{d}C_1} = -\frac{(1-\beta)}{(1-k)}\left[1 + \frac{\boldsymbol{v}\cdot\nabla T}{\partial T/\partial t}\right]\frac{f_1}{C_1} \quad \cdots \quad (1)$$

where $f_1$ is the volume fraction liquid; $C_1$ is the solute concentration in the liquid in weight per cent; $\beta = (\rho_s - \rho_1)/\rho_s$ is the solidification shrinkage, in which $\rho_1$ and $\rho_s$ are the densities of the liquid and solid, respectively; $k$ is the partition coefficient; $\boldsymbol{v}$ is the liquid velocity vector; $\nabla T$ is the temperature gradient; and $\partial T/\partial t$ is the time rate of temperature change. The latter quantity can also be expressed in terms of the isotherm velocity vector $\boldsymbol{v}^{\mathrm{T}}$ and the temperature gradient as $\partial T/\partial t = -\boldsymbol{v}^{\mathrm{T}}\cdot\nabla T$. Then, the last term in the square brackets in equation (1) can be viewed as the local liquid velocity perpendicular to the isotherms, $v_{\mathrm{n}} = \boldsymbol{v}\cdot\nabla T$, relative to the normal isotherm velocity, $v_{\mathrm{n}}^{\mathrm{T}} = \boldsymbol{v}^{\mathrm{T}}\cdot\nabla T$.

The physical significance of equation (1) can be understood as follows (for $k < 1$):

1. Equation (1) reduces to the Scheil equation, implying no macrosegregation, when $\beta$ and $\boldsymbol{v}$ both vanish.

2. Equation (1) also reduces to the Scheil equation when the liquid velocity is just that required to feed solidification shrinkage, i.e. $v_{\mathrm{n}} = -v_{\mathrm{n}}^{\mathrm{T}}\beta(1-\beta) = v_{\mathrm{s}}$, where $v_{\mathrm{s}}$ is the shrinkage flow velocity perpendicular to the isotherms.

3. If the liquid velocity alone is zero, for example at an impenetrable chill face, but the shrinkage $\beta$ is finite ($>0$), positive macrosegregation will result; this is the so called inverse segregation often observed in casting of aluminium alloys.

4. Flow in the same direction as the shrinkage flow (i.e. in the direction of decreasing temperature), but with a speed *greater* than the shrinkage velocity, i.e. $v_{\mathrm{n}} < v_{\mathrm{s}}$, results in negative macrosegregation.

5. Both flow in the same direction as the shrinkage flow, but with a speed *less* than the shrinkage velocity, as well as flow in the opposite direction (in the direction of increasing temperature, towards regions of lower solid fraction), i.e. $v_{\mathrm{s}} < v_{\mathrm{n}} < v_{\mathrm{n}}^{\mathrm{T}}$, result in

positive macrosegregation. Examples include centre-line and under-riser segregation in steel casting.

6. If the flow velocity in the direction of increasing temperature is larger than the isotherm velocity, i.e. $v_n > v_n^T$, the term in the square brackets in equation (1) becomes negative and local remelting results. This is the cause of the open channels in the mush that lead to A segregates or freckles.

Mehrabian *et al.*[8] proposed that the interdendritic flow velocities could be calculated from Darcy's law for flow in porous media

$$\boldsymbol{v} = -\frac{K}{\mu f_1}(\nabla P - \rho_1 \boldsymbol{g}) \quad \ldots \ldots \ldots \ldots (2)$$

where $K$ is the permeability; $\mu$ is the viscosity; $\nabla P$ is the pressure gradient; $\rho_1$ is the density of the liquid as in equation (1); and $\boldsymbol{g}$ is the gravity vector. Piwonka and Flemings[9] and Apelian *et al.*[10] were the first researchers to perform experiments to measure the permeability of mushy zones as a function of the liquid fraction, and microstructural parameters such as dendrite arm spacings.

Flemings and co-workers applied the above model to various alloys and casting situations, in order to predict typical macrosegregation patterns and verify them experimentally. For example, Mehrabian *et al.*[11] predicted the conditions for freckling, and Kou *et al.*[12] predicted the conditions for freckling in rotating, axisymmetric ingots. Early work by Mehrabian and Flemings[13] on ternary alloys was extended in the late 1970s by Fujii *et al.*[14] to macrosegregation in multi-component low alloy steels. Fujii *et al.* solved the coupled equation set given by the LSRE and Darcy's law, but the temperature field was taken from measurements. A shortcoming of all the above studies is that they neglect flow in the (fully melted) bulk liquid region ahead of the mushy zone.

The first macrosegregation model that accounted for the coupling of the flow between the mushy and bulk liquid zones was reported by Ridder *et al.*[15] in the early 1980s. Ridder *et al.* solved the coupled set of equations given by Darcy's law, the energy equation, and the LSRE in the mushy zone, and the momentum and energy equations in the fully liquid region. Solutal convection in the bulk liquid was neglected. Predicted macrosegregation patterns compared favourably with experimental measurements. In the numerical solution of the equations, a two domain approach was employed, where boundary conditions were explicitly satisfied at the boundary between the mushy and bulk liquid zones, and each region was meshed separately. Because they considered a quasisteady system, the grid did not evolve with time.

## Applications of macrosegregation models

Modelling of macrosegregation made significant progress in the mid-1980s and early 1990s when so called *single domain models*, which are based on mixture theory or volume averaging,[16–18] were derived by Bennon and Incropera,[19] Beckermann and Viskanta,[20] Voller *et al.*,[21] and Poirier and co-workers.[22,23] These models consist of a set of mass,

momentum, energy, and solute conservation equations that are equally valid in the solid, mushy, and liquid regions of alloy solidification systems. Hence, the equations can be solved using a single domain, fixed numerical grid. The LSRE of Flemings and co-workers, equation (1), can be derived from the single domain models as a limiting case. The momentum equations are a generalisation of Darcy's law, equation (2), and reduce to the single phase Navier–Stokes equations in the liquid region. The numerical results obtained in these early studies illustrate the importance of the coupling of the flow between the mushy and liquid zones, and reveal the existence of complex thermosolutal convection patterns in the melt. In particular, Bennon and Incropera[24] and, later, Felicelli *et al.*[25] presented the first direct numerical simulations of freckles or A segregates.

Single domain continuum or volume averaged models have been further developed and used by numerous researchers. Articles by Beckermann and Viskanta,[26] Beckermann and Wang,[1] Prescott and Incropera,[2] and Combeau *et al.*[3] thoroughly review the very substantial body of literature on this subject, present the detailed derivations of the governing equations, and discuss laboratory scale experimental validation. The review by Worster[27] illustrates the strong interest of the fluid mechanics community in the same subject. Voller and co-workers[28–30] studied issues associated with numerical solutions of the governing equations. Instead of providing another comprehensive summary of this research, the remainder of this section is devoted to reviewing six recent applications of macrosegregation models to industrially relevant casting processes. These examples are intended to illustrate the present state of the art in modelling macrosegregation in a few selected casting processes and to highlight some of the shortcomings. It is emphasised that macrosegregation models have been applied to casting processes other than those covered in the examples below.

### Example 1: Steel ingot

The first example involves prediction of the classical macrosegregation pattern in a heavy steel ingot, as shown schematically in Fig. 3.[31] Negative segregation appears as a zone in the bottom third of the ingot. It is usually associated with equiaxed dendrites, formed early in the solidification process and relatively poor in solute, that have settled in this region. Positive segregation near the centreline, and particularly at the top (hot top segregation), arises partially from buoyancy- and shrinkage-driven interdendritic fluid flow during the final stages of solidification. The A segregates are pencil-like chains of equiaxed crystals that are highly enriched in solute. They are the result of buoyancy driven convection through the columnar dendritic zone in the same direction as, but at a faster speed than, the isotherm velocity, which causes local remelting (*see* item 6 in the list below equation (1)). The pencil-like shape of the A segregates is related to the localised nature of the thermosolutal convection patterns. During solidification, highly enriched melt from colder regions in the mush streams through the still open channels into the bulk liquid ahead of the
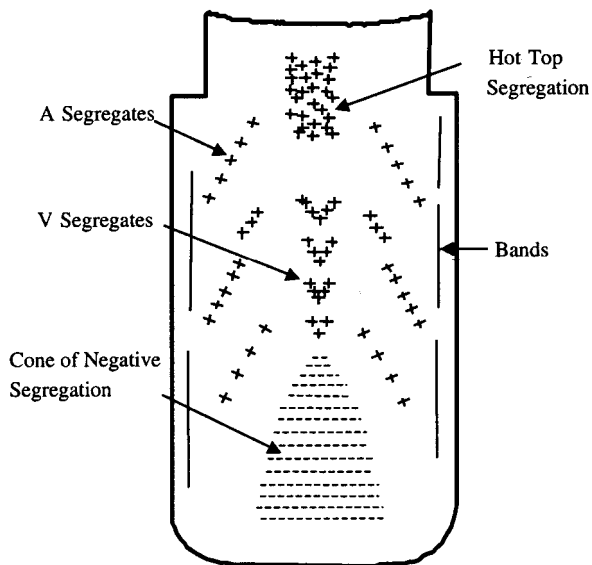
**3   Schematic of macrosegregation pattern in steel ingot (after Ref. 31)**

mushy zone. Hence, the bulk liquid is continually enriched due to the formation of A segregates, ultimately resulting in strong positive macrosegregation in the last region of the ingot to solidify (i.e. the top centre portion). The V segregates in the centre of the ingot arise from equiaxed crystals settling in the core

and forming a loosely connected network that can easily rupture due to metallostatic head and liquid being drawn down to feed solidification shrinkage. Fissures then open up along shear planes oriented in a V pattern, and are filled with enriched liquid. Finally, the banding pattern along the sidewalls of the ingot is believed to be due to unsteady heat transfer or flow early in the solidification process.

Gu and Beckermann[32] recently developed a single domain macrosegregation model for a steel ingot. The model considers eleven alloying elements in the steel, including their different segregation behaviours and effects on the liquid density. The highly coupled advection–diffusion equations in the model were discretised on a two-dimensional (2D) rectangular grid using the finite volume method. The mould geometry and thermal boundary conditions were patterned after an experimental ingot, about 2·55 m in height, cast at Lukens Steel Company. Results for the predicted evolution of the solid fraction and liquid velocity distributions are shown for four different times in Fig. 4. Strong buoyancy driven flow persists throughout the solidification process. Measured and predicted macrosegregation profiles at the vertical ingot centreline are compared in Fig. 5 for carbon and sulphur. While the level and variation of the macrosegregation is generally predicted well, the increase of carbon content in the melt, due to absorption of carbon from the insulation material, leads to an underprediction of the measured positive carbon



(a)          (b)          (c)          (d)
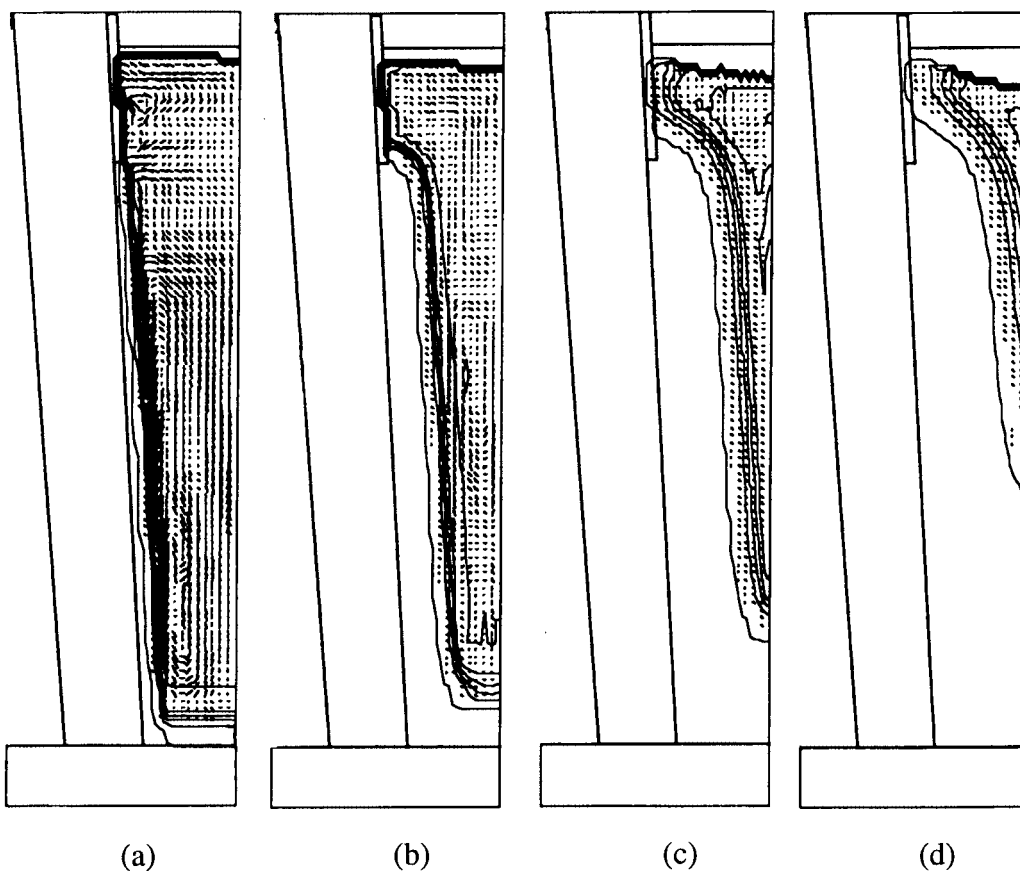
*a* 500 s; *b* 3000 s; *c* 9000 s; *d* 15 000 s

**4   Predicted velocity vectors (largest vector represents 2·5 cm s$^{-1}$) and solid fraction contours (in 20% increments) during solidification of 2·55 m (height) steel ingot[32]**
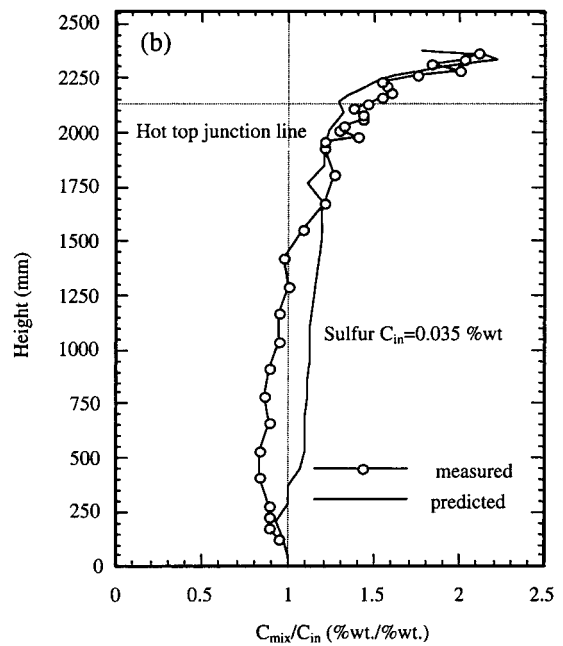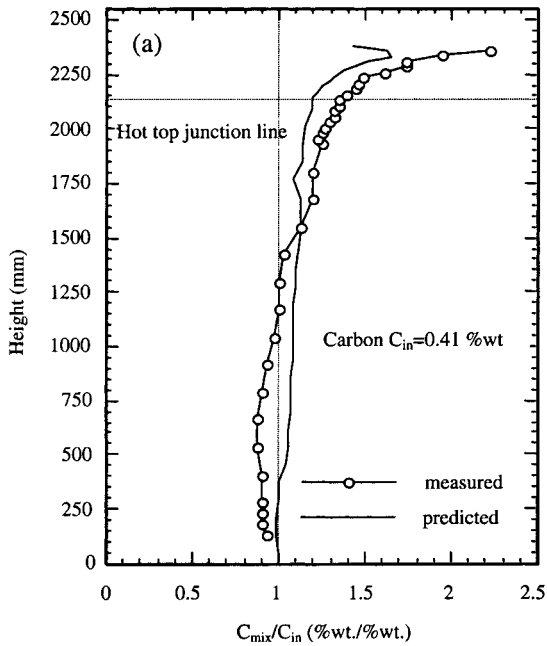
a carbon; b sulphur

**5  Comparison of measured and predicted macrosegregation variations along vertical centreline of steel ingot:[32] $C_{mix}$ and $C_{in}$ are local mixture concentration and initial concentration in ingot, respectively**

macrosegregation near the very top; no such disagreement exists for sulphur. The neglect of the movement of equiaxed crystals in the model prevents the prediction of V segregates along the vertical centreline. This may contribute to the underprediction of the measured negative macrosegregation over the middle half of the ingot. A corresponding underprediction of the positive macrosegregation can be observed near the hot top junction. Not shown here is the fact that the model also failed to predict the off-centreline A segregates (*see* Fig. 3) observed in the experimental ingot. This can be directly attributed to the coarse numerical grid used in the simulations. Similar observations were made by Vannier *et al.*[33] in their simulation of macrosegregation in a steel ingot. An earlier numerical study using a finer grid and a smaller domain readily predicted A segregates for a low alloy steel.[34] The failure to predict A segregates will also contribute to the underprediction of the positive macrosegregation near the hot top junction.

In summary, this study[32] revealed a number of shortcomings in macrosegregation modelling for a large steel ingot that are not easily overcome. The computational resources required to resolve flow patterns associated with A segregates (i.e. on a scale of a few millimetres) over an ingot about 2·5 m in height and solidifying over more than 10 h will probably be unavailable for at least the next decade. Gu and Beckermann[32] report a CPU time of 'several weeks' on an HP J200 single processor workstation for a grid of only 54 (height) × 38 (width) control volumes and time steps of the order of several seconds. Furthermore, three-dimensional (3D) effects and uncertainties in the mushy zone permeability may contribute to some of the disagreement between the measured and predicted macrosegregation patterns. A three-dimensional model of macrosegregation in

steel ingots (considering carbon and sulphur only) was recently reported by Sundarraj and Miller,[35] and much better agreement with the measured macrosegregation patterns of Ref. 32 was obtained. They claim to have achieved a mesh independent solution with 20 (height) × 12 (width) × 12 (thickness) control volumes. The total computational time was on the order of 5 h on a SGI workstation (200 MHz R4400 processor).[35]

With respect to the neglect of sedimentation of crystals in the model of Gu and Beckermann,[32] the reader is referred to an earlier study by Olsson *et al.*[36] They used experimental information from two steel ingots where the composition was varied to obtain different convection patterns in the mushy zone. This enabled them to distinguish between the effects of melt flow and of sedimentation of crystals on macrosegregation. They developed a simple equation that predicts the negative macrosegregation due to sedimentation of crystals as a function of the relative height of the sediment zone and the fraction of solid in that zone. They also noted that the LSRE, equation (1), might not be valid for large steel ingots because the distance between the free crystals is so large that the assumption of a well mixed liquid in equilibrium with the solid does not hold. The issue of macrosegregation in the presence of undercooled liquid is addressed in more detail below in the section 'Coupled microstructure–macrosegregation models'. Olsson *et al.*[36] also developed a phenomenological model of macrosegregation due to A segregates and obtained good agreement with measurements.

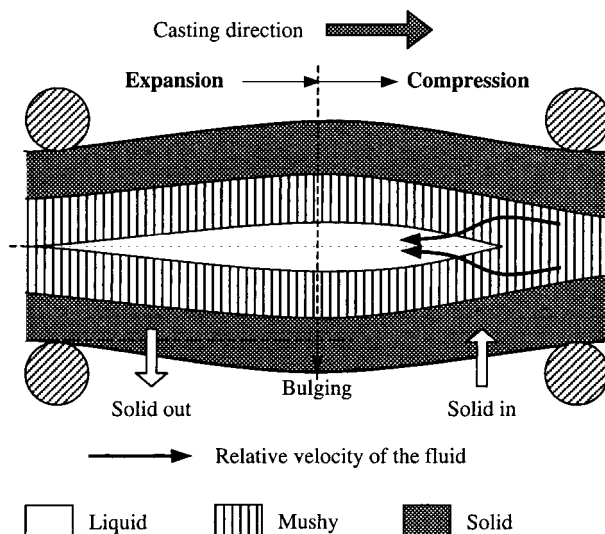## Example 2: Continuous casting of steel

Many of the macrosegregation patterns in continuous casting of steel are similar to ingot casting, if time is
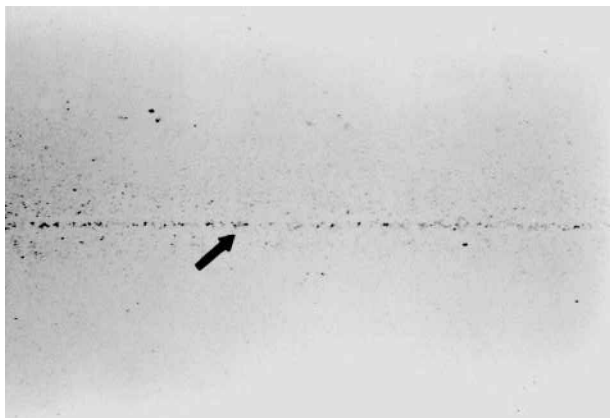
**6  Sulphur print showing centreline segregation in continuously cast steel slab: segregated centreline is no more than few millimetres in width (courtesy of Ipsco Inc.)**



**7  Schematic illustration of how bulging and compression of mush between two successive rolls during continuous casting of steel causes relative liquid–solid flow and, hence, macrosegregation (taken, with permission, from Fig. 1 in Ref. 38)**

measured with respect to a reference frame that moves with the strand.[37] A and V segregates, although less pronounced, may be seen in longitudinal sections of continuously cast steel. A sulphur print showing a typical macrosegregation pattern in a continuously cast steel slab is shown in Fig. 6. Here, the only obvious feature is the narrow band of strong positive macrosegregation along the centreline. This centreline segregation is often thought to be caused by bulging of the slab due to inadequate roll containment close to the bottom of the liquid pool, where the ferrostatic pressure is sufficiently large to cause creep of the solid crust. Figure 7 illustrates how bulging between two successive rolls of a continuous casting machine induces the necessary relative liquid–solid velocities.[38] Heat extraction results in growth of the mushy zone between the rolls. This mush must be compressed as the second roll is approached. As the solid network compacts, enriched liquid is expulsed from the mush, like during compression of a sponge.[39] The liquid flows toward regions of lower solid fraction (i.e. the liquid zone in Fig. 7), and thus causes positive macrosegregation near the centre of the slab. In addition to bulging, thermal contraction of the solid as it cools has also been identified as an important mechanism in macrosegregation formation in continuous casting of steel billets and blooms.[40] Hence, in order to predict macrosegregation in continuous casting of steel, the strains and deformations in the solid shell and of the solid inside the mushy zone must be taken into account, in addition to solidification shrinkage flows, melt convection, and sedimentation of free crystals. Such a comprehensive model does not exist; however, promising attempts are reviewed below.

Several studies modelling macrosegregation formation in continuous casting of steel have been reported for situations where bulging and solid deformation are not important. Aboutalebi *et al.*[41] (2D axisymmetric), Yang *et al.*[42] (3D), and Lee *et al.*[43] (3D) employed standard single domain macrosegregation models that solve the coupled mass, momentum, energy, and species conservation equations. All three studies included thermosolutal convection and a $k$–$\varepsilon$ turbulence model. Yang *et al.* accounted for multiple

species, whereas Aboutalebi *et al.* and Lee *et al.* focused on binary Fe–C alloys. Lee *et al.*[43] also included solidification shrinkage flow, motion of solid below a certain critical solid fraction (using a relative viscosity concept[44]), and the effect of soft reduction. All three studies claim good correspondence between measured and predicted macrosegregation patterns. None of the studies accounts for the presence of a columnar to equiaxed transition (CET) in the structure of the castings simulated. Choudhary and Gosh[45] measured considerable macrosegregation at the location of the CET, in addition to the centreline macrosegregation, in continuously cast steel billets. This indicates a strong correlation between the grain structure and macrosegregation. Settling of free equiaxed grains can also contribute to macrosegregation, as already mentioned in connection with stationary ingot casting.

Interesting theoretical approaches to the problem of macrosegregation due to solid deformation were developed by Lesoult and Sella[39] and Fredriksson and co-workers.[46,47] They modified the LSRE, equation (1), to account for changes in the volume of the mush element in Fig. 2 due to interdendritic strains and deformation of the solid skeleton. None of these studies considers bulging; instead, they concentrate on the thermal strains due to differential contractions during cooling. Lesoult and Sella[39] and Raihle and Fredriksson[46] were able to explain the formation of positive centreline segregation due to contractions. El-Bealy and Fredriksson[47] and El-Bealy[48] obtained excellent agreement between measured and predicted fluctuating macrosegregation patterns near the cast surface due to unsteady heat extraction in the primary and secondary cooling zones of a continuous slab caster. In these studies, the conservation equations were not fully coupled, and El-Bealy and Fredriksson solved their modified LSRE only in one dimension across the slab thickness.

A more complete model of macrosegregation in continuously cast steel billets and blooms that considers thermal deformations of the solid only (and not bulging) was developed by Janssen *et al.*[49] within the framework of a two phase computational fluid dynamics code (Phoenics). Whereas Lesoult and Sella[39] express their governing equations in a Lagrangian form, Janssen *et al.*[49] use a more common Eulerian formulation. Only solid deformation in the thickness direction across the mushy zone was taken into account. The solid velocities were obtained by requiring that the product of the solid density and velocity is a constant and taking the solid density as a function of temperature. They obtained good qualitative agreement between calculated and measured radial macrosegregation profiles for carbon and phosphor in a bloom.

Miyazawa and Schwerdtfeger[50] developed an early model of macrosegregation due to bulging and contractions in continuously cast steel slabs, by solving combined mass and species conservation equations together with Darcy's law. Between pairs of support rolls, where the strand bulges, the dendrites are assumed to move with the same velocity as the solid shell. In the region where the strand is squeezed together (i.e. at each pair of support rolls), the solid phase is assumed to move with a horizontal velocity that depends linearly on the solid fraction. Miyazawa and Schwerdtfeger obtained good qualitative agreement with macrosegregation profiles observed in practice. A similar approach, where the velocity of the solid phase due to bulging is prescribed through simple algebraic relations, has been used in combination with a two-dimensional, two phase, single domain mixture model by Ohnaka and Shimazu[51] to predict measured macrosegregation profiles in continuously cast steel slabs.

The most advanced model to date of deformation induced macrosegregation in the continuous casting of steel has been presented very recently by Kajitani *et al.*[38] Based on two-dimensional heat flow calculations, the bulging of the slab between pairs of support rolls was first simulated using the Abaqus code, while neglecting thermal contractions. The solid velocities across the deforming mushy zone were then obtained by using the bulging profile as input and assuming a linear variation between the solidus isotherm and the centreline in the compression areas. The solute conservation equation, Darcy's law, and a mass conservation equation that accounts for shrinkage were solved together iteratively. Figure 8 shows typical carbon macrosegregation profiles computed by Kajitani *et al.*[38] It can be seen that the solute content along the centreline increases with each bulging event, while shrinkage flows alone cause a slight reduction (Fig. 8a). The macrosegregation profiles after six rolls across the slab thickness, shown in Fig. 8b, indicate that bulging alone results in strong positive segregation near the centre and negative segregation in the peripheral regions of the slab, whereas shrinkage alone results in an opposite behaviour. Together, bulging and shrinkage produce strong positive segregation at the centre, negative segregation in the periphery, and a second negative zone adjacent to the positive centreline segregation. No direct com-
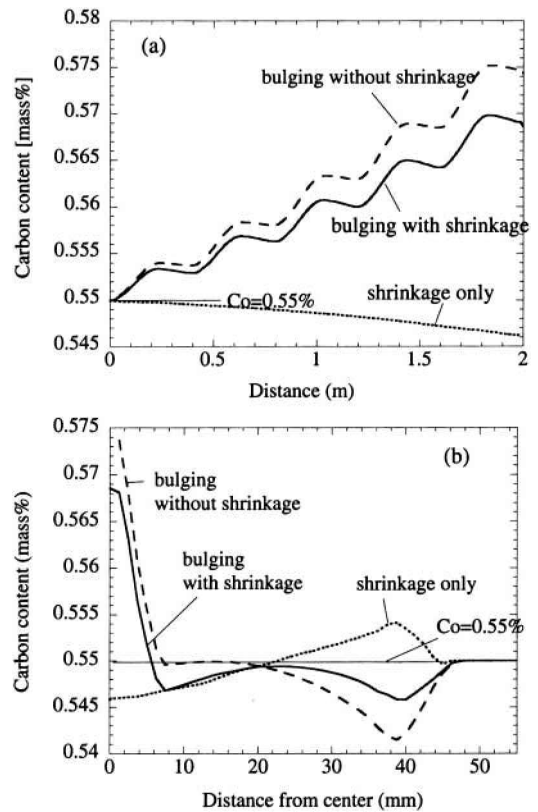


*a* along centreline (distance between rolls is 400 mm); *b* across slab thickness after six rolls ($f_s = 0.37$ at centreline, maximum bulging of 0.1 mm)

**8   Predicted macrosegregation patterns during continuous casting of steel: $C_o$ is initial carbon content (with permission from Ref. 38)**

parisons with experiments were offered by Kajitani *et al.*,[38] owing in part to convergence problems at low and high solid fractions. It was noted that improved descriptions are needed for the deformation behaviour of the solid skeleton in the mushy zone, particularly when the solid fraction is high and coherency is increased by coalescence of neighbouring columnar dendrite branches. The model should also be improved by accounting for the inner equiaxed zone usually present in continuous casting of steel. The deformation behaviour of a mush consisting of equiaxed grains can be expected to be different from that of a columnar structure.

## Example 3: Aluminium direct chill casting

The next example deals with macrosegregation in direct chill (DC) casting of aluminium alloys. Typical macrosegregation patterns have been measured by Finn *et al.*[52] for Al–4·5 wt-%Cu cylindrical ingots solidified both with and without grain refiner, as illustrated in Fig. 9. Finn *et al.* showed that, for the grain refined ingot with an equiaxed structure, the mushy zone is *more* permeable and allows for advection (by buoyancy driven flow) of solute rich liquid toward the centreline, thus producing *positive* centreline macrosegregation. On the other hand, in the case without grain refiner (columnar structure), the *less* permeable mush reduces such advection, and the
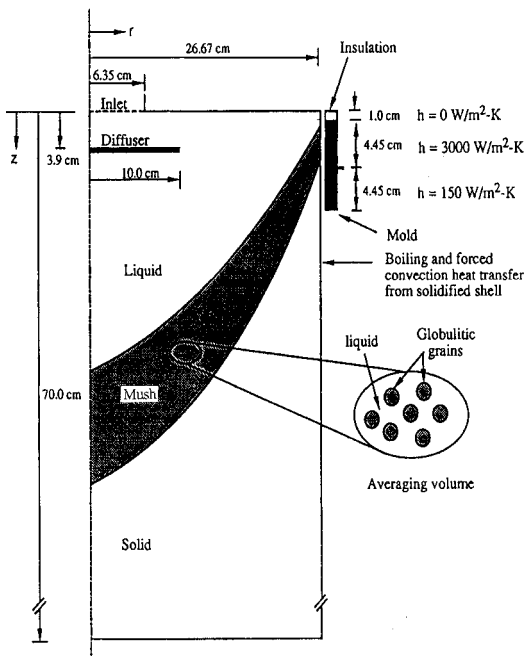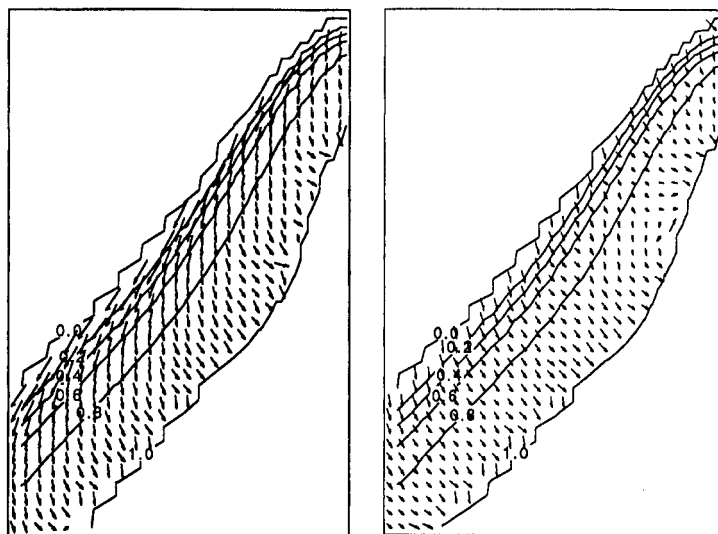
*a* schematic illustration of simulation domain (*h* is heat transfer coefficient); *b, c* predicted relative velocities and solid fraction contours (from 0·0 to 1·0 in intervals of 0·2) inside mushy zone near mould for simulations with and without grain refiner, respectively

**9 Simulation of direct chill (DC) casting of Al–4·5 wt-%Cu cylindrical ingot[53]**

remaining shrinkage driven flow produces *negative* centreline segregation. In both cases, strong positive macrosegregation due to shrinkage driven flow and exudation was measured at the ingot surface.

Results from numerical simulations of these experiments are shown in Figs. 9 and 10.[53] Close-ups of predicted relative liquid velocities and solid fraction contours inside the mushy zone are shown in Fig. 9*b* and 9*c* for the grain refined and non grain refined cases, respectively. In both cases, it can be seen that there exists a shrinkage driven flow towards the eutectic front. In the grain refined case (Fig. 9*b*), with a more permeable mushy zone, a relatively strong thermosolutal buoyancy driven flow towards the ingot centreline is present in the lower solid fraction region of the mush. As measured in the experiments, the simulations showed that the buoyancy driven flow in the grain refined case produces positive centreline macrosegregation (Fig. 10*a*). On the other hand, in the non grain refined case, the shrinkage driven flow, together with the weakness of the buoyancy driven flow, results in negative centreline macrosegregation (Fig. 10*b*). Because exudation was neglected, the extent of positive inverse segregation at the ingot surface is somewhat underpredicted. Surface macrosegregation in aluminium DC casting has been modelled successfully by Mo and co-workers.[54–58]

The above comparison shows that the macrosegregation model predicts the correct macrosegregation trends and magnitudes, and illustrates the strong effect of the microstructure. However, the grain sizes and dendrite arm spacings needed in the permeability model were taken from the experiments. A truly predictive model would also need to predict the
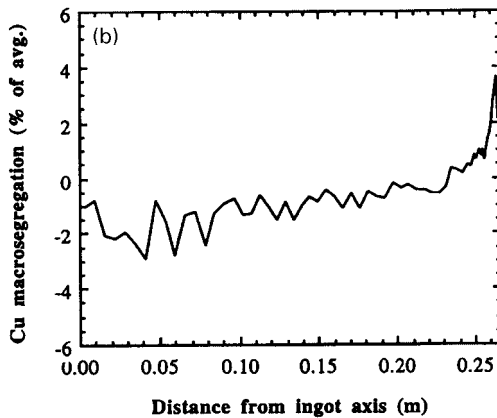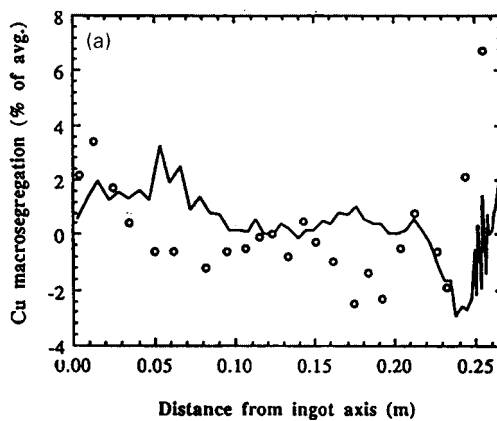


*a* comparison of measured and predicted profiles in grain refined experiment of Finn *et al.*;[52] *b* predicted profile in simulation without grain refiner

**10 Radial macrosegregation profiles in DC casting of Al–4·5 wt-%Cu cylindrical ingot[53]**
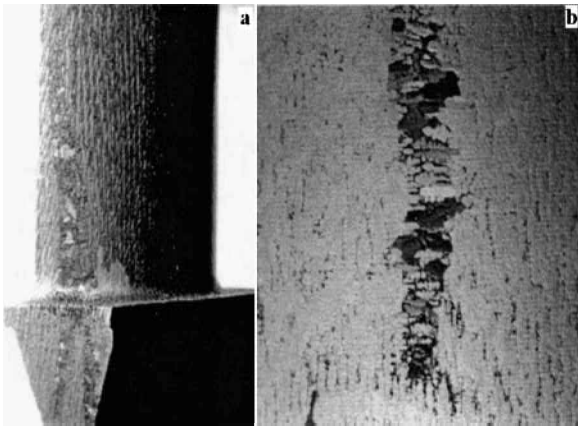
11 *a* freckles in single crystal Ni base superalloy prototype blade and *b* higher magnification of single freckle: freckles are about 1–2 mm wide (courtesy A. F. Giamei, United Technologies Research Center)

microstructure. Furthermore, it has been argued that the transport of broken/detached solid fragments and equiaxed grains from the mould region to the ingot centre tends to cause negative centreline macrosegregation in aluminium ingots (*see* e.g. Ref. 59). Preliminary simulations with a two phase model support this conclusion.[60] The effect of free floating dendrites on macrosegregation in DC casting of aluminium alloys has also been modelled recently by Vreeman and co-workers.[61,62] Further discussion regarding the modelling of macrosegregation in the presence of moving equiaxed dendrites can be found in a subsequent section. None the less, simulation of the transport phenomena during solidification of the complex multicomponent alloys used in actual DC casting processes,[63] concurrently with the prediction of grain structure development, is still lacking. Coupled macrosegregation and grain structure measurements for a commercial DC cast 5182 aluminium alloy, suitable for validation of such future models, have recently been reported by Joly *et al.*[64]

## Example 4: Single crystal nickel base superalloy casting

A particularly severe and technologically important macrosegregation phenomenon is freckling in directional solidification of single crystal nickel base superalloys. Components with freckles are rejected. Figure 11 shows photos of such freckles in an experimental superalloy casting. During solidification of nickel base superalloys, a number of light elements (such as aluminium and titanium) are rejected into the liquid, and some heavy elements (such as tungsten) are preferentially incorporated into the solid, leading to strong solutal buoyancy forces in the mushy zone. Despite the presence of a stabilising thermal gradient, these buoyancy forces can trigger convection cells, leading to open channels in the mush through which liquid streams upwards into the superheated region of the mould. The remelting necessary to generate open channels occurs according to the mechanism mentioned in the sixth item discussed in connection with the LSRE, equation (1). The channels are con-
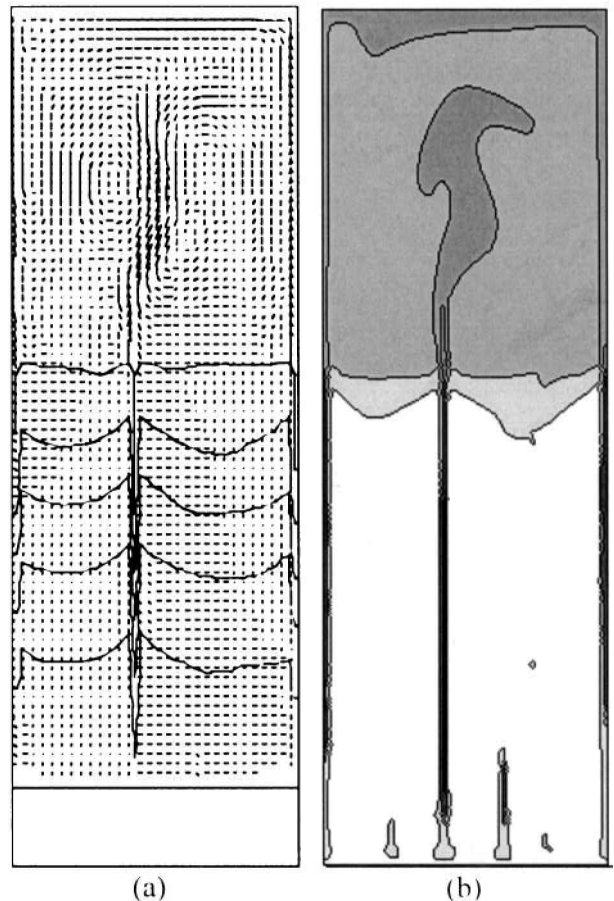


12 *a* predicted velocity vectors (largest vector represents 6·3 mm s$^{-1}$) and solid fraction contours (in 20% increments) and *b* macrosegregation pattern (Ti concentration normalised by initial concentration in equal intervals between 0·87 and 1·34) showing freckle formation during upward directional solidification of single crystal Ni base superalloy in 5 × 15 cm rectangular domain[65]

tinually fed by melt flow through the surrounding mush. Later, these channels are filled with dendrite fragments, which are then observed as freckle-like chains of equiaxed crystals in the otherwise single crystal columnar structure.

Typical predictions of freckling in upward directional solidification of a superalloy from a two-dimensional micro-/macrosegregation model[65] are presented in Fig. 12. The novel feature of this model is that phase equilibrium was calculated at each time step, using a thermodynamic subroutine for multicomponent nickel base superalloys. The open channels in the mush through which enriched liquid streams upward into the bulk melt are predicted realistically. The filling of these channels with equiaxed grains, leading to the appearance of freckles in a fully solidified casting, has recently been simulated by Gu *et al.*[66] Simulations of freckling in directional solidification of superalloys have also been performed by Felicelli *et al.*,[67–69] using a finite element method, and by Combeau *et al.*[3] using a finite volume method.

Although three-dimensional calculations have been reported by Neilson and Incropera[70] and Felicelli
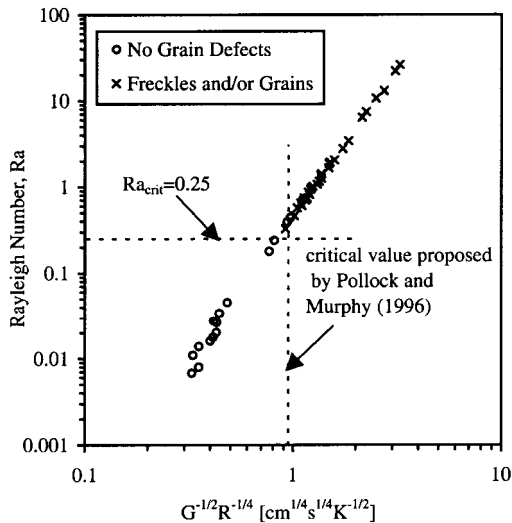
**13 Variation of mush Rayleigh number with local thermal conditions in experiments of Pollock and Murphy[74] on directional solidification of single crystal Ni base superalloys: no freckles form below critical mush Rayleigh number of 0·25 (Ref. 73): *G* and *R* are temperature gradient and isotherm speed, respectively**



**14 Simulation results for dependence of critical mush Rayleigh number on inclination of domain with respect to gravity for freckle initiation in directional solidification of single crystal Ni base superalloys[73]**

*et al.*,[71,72] extension of such simulations to actual cast components is difficult, due to the large computer resources required to resolve such small macrosegregation features over the scale of the entire component. For this reason, a simpler freckle predictor was developed that relies on the calculation of a local mush Rayleigh number in casting simulations that consider heat transfer only.[73] This Rayleigh number is based on the mean permeability and the liquid density inversion over the height of the mush zone.[27] Figure 13 shows the variation of the Rayleigh number with the local thermal conditions (temperature gradient and isotherm speed). The symbols in Fig. 13 correspond to the experiments of Pollock and Murphy.[74] Based on their measurements of freckle occurrence, a critical Rayleigh number for freckle formation can be identified. The critical Rayleigh number derived from experiments agrees with the value corresponding to freckle initiation in the simulations. Figure 14 shows how additional simulations can then be used, instead of experiments, to determine the variation of the critical Rayleigh number with the inclination of the casting with respect to gravity.[73] Very recently, Auburtin *et al.*[75] performed experiments on freckle formation in superalloy castings at various angles to the vertical, and also developed a freckle criterion that shows good correlation with their data. The modelling results of Ref. 73 and the experimental data of Ref. 75 still need to be reconciled.

## Example 5: Casting of metal matrix composites

Macrosegregation is also of concern in the casting of metal matrix composites (MMCs). Mortensen and co-workers[76–79] developed a model and performed experiments for unidirectional pressure infiltration of a fibrous preform by a binary Al–Cu alloy. In this
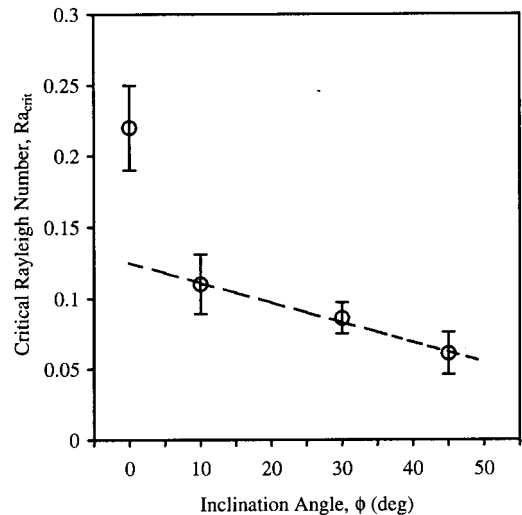
process, the alloy that first solidifies on the fibres is low in solute. Continued infiltration then forces the remaining solute rich liquid past the fibres that already have a solid layer on them, resulting in solute enrichment downstream of the path followed by the infiltration front. This, in turn, leads to macrosegregation in the matrix of the cast composite, with the largest positive macrosegregation observed at the last infiltrated point in the mould. The macrosegregation pattern predicted by Mortensen and co-workers was in good agreement with their experimental measurements.

Feller and Beckermann[80] investigated macrosegregation and particle redistribution during solidification of metal matrix particulate composites (MMPCs). In casting of MMPCs, the reinforcing particles (e.g. SiC or graphite) are dispersed into the liquid alloy (typically aluminium alloys) before introduction into the mould and solidification. The particles may be segregated to different regions of the casting due to settling/floating, as well as due to interactions with the advancing mushy zone. This is illustrated for the rectangular domain modelled in Ref. 80 in Fig. 15. The three phase (i.e. solid–particle–liquid) model developed by Feller and Beckermann assumes that the solid matrix is rigid and stationary at all times, whereas the particles in the single phase liquid region are generally mobile. It is also assumed that the particles are entrapped by the advancing dendrites, and that no particle rejection occurs at the interface between the mushy zone and the liquid region.

In order to illustrate the effect of the particles on macrosegregation, sample simulation results from the study of Feller and Beckermann[80] are shown in Figs. 16 and 17. Simulations were conducted for solidification of an Al–7 wt-%Si alloy with SiC particles inside the cavity shown in Fig. 15. Three cases were considered: no particles (case I); 20 vol.-% particles with a diameter of 14 μm (case II); and 20 vol.-% particles with a diameter of 100 μm (case III).
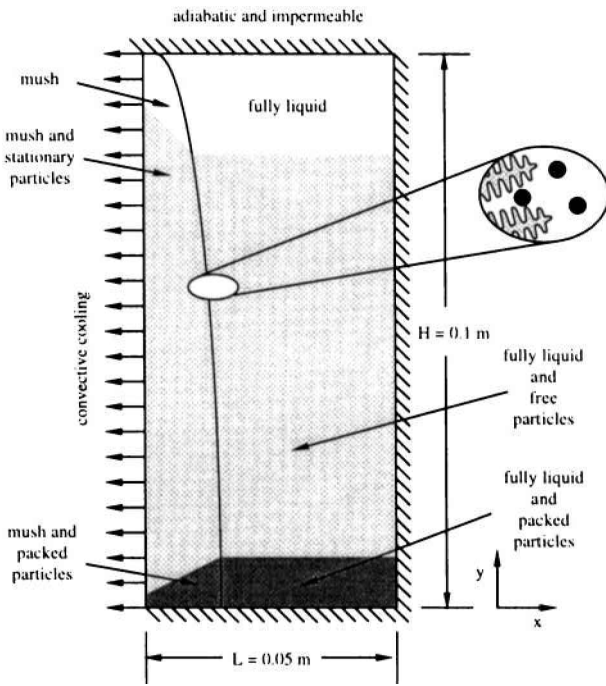
**15 Schematic illustration of domain and boundary conditions used in simulation of solidification of Al–7 wt-%Si metal matrix composite with SiC particles: different degrees of shading indicate particle concentration at intermediate time[80]**

Figure 16 shows the computed bulk solid fraction, defined as the sum of the solid and particle volume fractions, and liquid velocity fields at an intermediate time during solidification. It can be seen that the liquid velocities in case II, with the small particles, are much smaller than in case I, without particles. This can be explained by the fact that the melt–particle mixture viscosity is more than twice as high as the melt viscosity without particles. Furthermore, very little particle settling occurs in case II, as witnessed by the uniformity of the bulk solid fraction in the solid free region, because the relative velocity between the particles and the liquid is very small for the 14 μm particles. In case III, the large size of the particles (100 μm) results in much greater relative velocities. Consequently, the lower third of the cavity in Fig. 16c contains a packed bed of particles that settled before the mush could entrap them. The upper half of the cavity is virtually free of particles in case III, and melt velocities in this region are of a magnitude similar to those in case I.

The computed macrosegregation patterns (of silicon) at the end of solidification are shown in Fig. 17 for all three cases.[80] For the unreinforced alloy in case I, macrosegregation is widespread, with strong positive segregation present along the insulated walls of the cavity (bottom and the right-hand walls), and several channel segregates present in the centre. This macrosegregation is caused by thermosolutal convection. On the other hand, for cases II and III
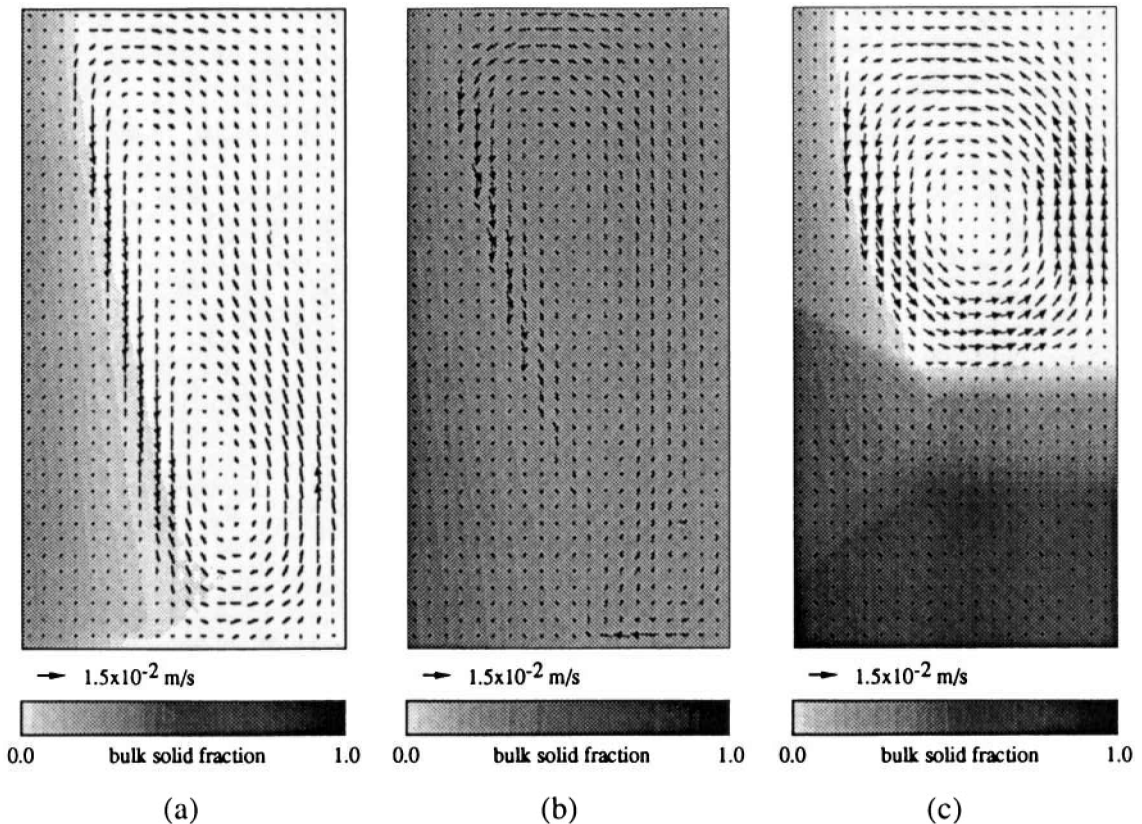


*a* case I (unreinforced); *b* case II (small particles); *c* case III (large particles)

**16 Predicted bulk solid fraction (particle plus solid matrix) distribution and liquid velocity vectors during solidification of metal matrix particulate composites in domain shown in Fig. 15 (Ref. 80)**
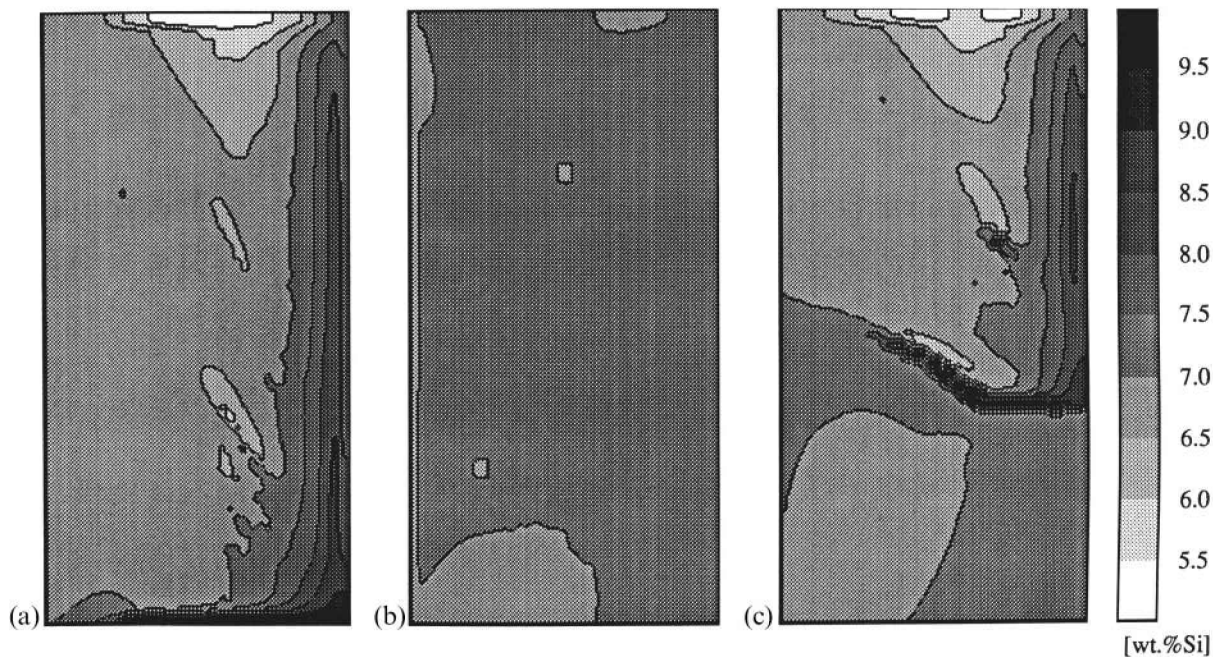
*a* case I (unreinforced); *b* case II (small particles); *c* case III (large particles)

**17 Predicted final macrosegregation patterns for solidification of metal matrix particulate composites in domain shown in Fig. 15 (Ref. 80)**

(i.e. with particles), macrosegregation is negligible when reinforcement is present. This can be explained by the reduction in the convection velocities due to the presence of the particles. The particles not only increase the viscosity, but also strongly decrease the permeability in that portion of the mush where the solid fraction is low and the permeability would be high in the absence of particles. Convection in the low solid fraction portion of a mushy zone is the primary cause of macrosegregation in unreinforced alloys. Since the upper right-hand portion of the cavity is particle free in case III due to settling, the extent of macrosegregation in that region is similar to case I. Hence, macrosegregation can be prevented by the addition of small particles to the melt.

While the previous work succeeds in predicting a number of important phenomena relevant to macrosegregation in MMCs, there are numerous issues that deserve further research attention. Some of the issues still to be addressed include: (i) the effect of a nonstationary solid phase, especially if crystals nucleate on moving particles; (ii) particle rejection at the mush/liquid interface when the solid microstructure in the mush is relatively dense;[81] (iii) macroscopic particle movement within the low solid fraction portion of the mushy zone;[82] (iv) microstructural changes due to interactions between the matrix and the reinforcement;[83] and (v) rheological behaviour of the particle–melt mixture, especially when it is non-Newtonian.[84] Certainly, additional experiments are needed to clarify these and other issues.

## Example 6: Complex steel casting

The final example illustrates that macrosegregation due to interdendritic flow can now be simulated for the complex shaped castings commonly encountered in foundry practice. A three-dimensional model was

developed[85] based on the formulation for macrosegregation formation in multicomponent steel of Ref. 34. In order to reduce the computational effort, the solid fraction as a function of temperature was specified as model input, instead of calculating it from the temperature–concentration coupling in the mushy zone through phase equilibrium. In addition, shrinkage driven flow and solid movements were neglected. The governing equations were discretised using a control volume based finite difference scheme. The pressure–velocity coupling was handled using either a modified version of the Sola-VOF algorithm or the Simplec scheme, depending on which scheme required less iteration in the previous time steps. Some limited experimental validation was presented for a simple block casting with a central top riser.[85]

Figure 18 shows an example of macrosegregation calculations for a large (96 300 kg, maximum dimensions 2·65 × 2·1 × 3·7 m) production steel casting poured in a green sand mould with an insulated riser and water cooling lines run through the hole in the centre of the casting.[85] One half of the casting was enmeshed with 113 760 control volumes of which 21 420 were metal volumes. A typical simulation took less than one day on a medium range computer workstation. Figure 18*a* is a plot of the predicted convection patterns in the bulk liquid and mushy zones during solidification. Particularly strong flow exists around the hole in the casting. Figure 18*b* shows the predicted carbon macrosegregation pattern in the fully solidified casting. It can be seen that the flow has created carbon rich regions around the hole and in the centre portion of the riser. These macrosegregation predictions have not yet been compared to measurements. It can be expected that the neglect of shrinkage driven flow in the model of Ref. 85 leads to some inaccuracies in the macrosegregation predictions, particularly at the riser/casting junction where
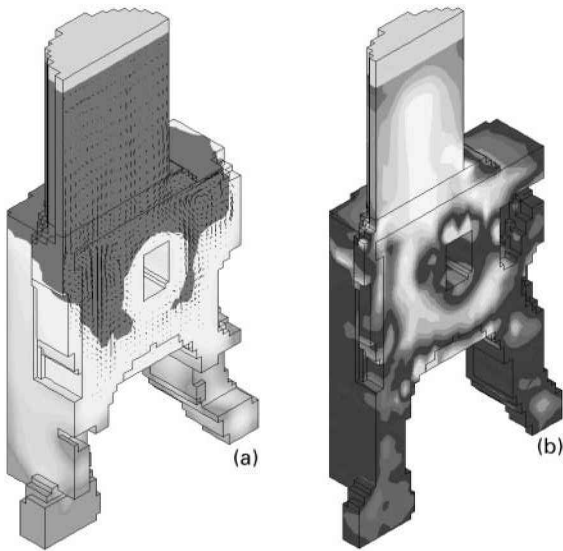
*a* predicted liquid velocity vectors (largest vector represents 1 cm s$^{-1}$) in mush (light shade) and liquid (dark shade) regions at time when casting is 50% solidified; *b* calculated final C macrosegregation pattern where concentrations range from 0·21 wt-%C (dark shade) to 0·25 wt-%C (light shade)

**18 Simulation of macrosegregation formation in large (2·65 m height) steel casting[85]**

the shrinkage flow velocities are largest. As in the steel ingot example, the resolution of small scale macrosegregation features (such as A segregates or freckles) in large castings is also beyond the current capabilities of the model of Ref. 85.

## Coupled microstructure–macrosegregation models

The examples in the previous section illustrate that the microstructure of castings, such as the dendrite arm spacings and the type of grain (i.e. columnar or equiaxed), has a profound influence on macrosegregation. Many macrosegregation features cannot be predicted without detailed consideration of the microstructure. Further progress in macrosegregation modelling can only be made if the microstructure is predicted as well. This section highlights recent efforts to develop coupled microstructure–macrosegregation models.

The most obvious example of this interdependency is the variation of permeability with microstructure. In directional solidification (i.e. columnar dendritic growth), the dendrite arm spacings are the primary microstructural parameters that affect the permeability, and much work has been performed to measure or calculate the permeability of such systems.[86–91] However, most castings (both continuous and static) feature zones of equiaxed grains, or are fully equiaxed. In the equiaxed case, both the grain density and the structure of individual grains influence the permeability. This was shown theoretically by Wang *et al.*,[92] and verified experimentally for aluminium alloys by Nielsen and co-workers.[93,94] Poirier and co-workers[95,96] also investigated this dependency of the permeability on the structure of equiaxed grains. Duncan *et al.*,[97] in their measurements of the

permeability of equiaxed Al–Cu alloys, accounted for the large influence of coarsening of the microstructure. They also noted that coarsening rates were enhanced by the melt flow. The situation is further complicated by the fact that small dendrite fragments or equiaxed grains can move in the melt before forming a coherent solid, resulting in macrosegregation by settling (or flotation). The drag coefficients of single equiaxed dendrites have recently been measured and correlated.[98] Wang *et al.*[92] provided a correlation for the interfacial drag in equiaxed solidification that covers the entire range from a single particle to a packed mush. Arnberg *et al.*[99] measured the coherency point in equiaxed solidification, when the dendrites start to impinge and form a continuous solid network. Even though much work has been performed to investigate the dependence of the permeability on the microstructure, the coupled prediction of the microstructure together with convection and macrosegregation is still lacking in many respects.

Different microstructures also result in different microscopic solute rejection (i.e. microsegregation) processes that, in turn, influence macrosegregation. It is well known that for a given alloy a finely dispersed microstructure promotes Lever rule type microsegregation behaviour, where both the solid and liquid are solutally well mixed and in equilibrium on the scale of the dendrite arms. On the other hand, a coarser microstructure, with less interfacial area per unit volume, tends to result in Scheil type microsegregation behaviour, where there is negligible solute diffusion in the dendrite arms. Since different amounts of solute are rejected into the interdendritic liquid depending on the microsegregation behaviour, different macrosegregation patterns will result in the presence of flow. Conversely, since macrosegregation changes the local average alloy composition, it will induce different microsegregation behaviours. The situation is further complicated by the fact that the dendrites in the mushy zone undergo considerable coarsening during solidification, implying that the microstructural length scale that controls microsegregation is not a constant. The topic of coupled micro-/macrosegregation has recently received much research attention (Refs. 34, 56, 65, 100–105), and can now effectively be dealt with, even for multicomponent alloys with different mass diffusivities for each solute. Some micro-/macrosegregation models have been developed for situations where multiple phases are forming, such as during eutectic and peritectic reactions or transformations.[106–111] None the less, there are often large uncertainties in the prediction of the microstructure that underlies the micro-/macrosegregation processes during solidification.

Furthermore, the melt must undercool before nucleation and growth of solid microstructures can proceed; however, all the previously reviewed macrosegregation models assume that the liquid is in equilibrium and locally well mixed (as in the Scheil or Lever rule models). In reality, all castings with equiaxed structures feature correspondingly large undercooled liquid regions during solidification. For example, M'Hamdi and co-workers[112,113] estimated that, in the continuous casting of steel, there is an undercooled liquid zone several metres in height. A

large undercooled zone has also been predicted for DC casting of aluminium.[60] Even in purely columnar growth, there is a potentially large undercooled liquid region in front of the primary dendrite tips, especially when the thermal gradient is low (such as in sudden cross-section expansions in casting of columnar turbine blades). Although the level of undercooling may be no more than a few degrees in traditional casting processes, its consideration is crucial when modelling coupled microstructure–macrosegregation development. During growth of dendrites or other structures in an undercooled melt, the microscopic solute rejection behaviour (and also the solid fraction variation) can be very different from that during solidification with a well mixed interdendritic liquid in equilibrium, which in turn influences macrosegregation. Several models of this effect have been developed for purely diffusive conditions where flow can be neglected.[114–120] Solute rejection from equiaxed dendrites growing and moving in an undercooled melt has been investigated experimentally by a few researchers.[121–124] Severe solute pluming was observed in the wake of the crystals. An example of a macrosegregation model that accounts for the growth of equiaxed grains in an undercooled melt is presented later in this section. No such models are available for other structures, such as columnar dendrites.

While it is beyond the scope of this work to present the details of the coupled microstructure–macrosegregation models that have been developed during the past decade, the remainder of this section briefly reviews their origin and then presents a single example of model predictions. The reader is referred to other reviews[1,2] for a thorough description of the models, including the derivation of the governing equations.

Modelling of microstructure formation in castings has been summarised by Rappaz,[125] Gandin *et al.*,[126] and Rappaz *et al.*[127] However, the only models to date that consider concurrent microstructure and micro-/macrosegregation development (including melt convection and grain movement) are the two phase model of Ni and Beckermann,[128] the multiphase/multiscale model of Wang and Beckermann,[129–131] and the extended continuum model of Ni and Incropera.[132,133] In the derivation of the models by Beckermann and co-workers, as well as of those by Poirier and co-workers[22,23] mentioned in the previous section, the microscopic (or point) conservation equations for each phase are formally averaged over a representative elementary volume (REV), such as that shown in Fig. 2. The averaging results in separate macroscopic conservation equations for each phase and averaged interface conditions that can be solved using a single domain approach for the entire casting. The key advantages of a formal averaging procedure are:

- The macroscopic variables, such as the average solute concentration in the solid in the REV, are exactly defined in terms of the microscopic profiles.
- Each term in the averaged equations has a clear origin, and terms accounting for the latent heat, permeability, nucleation rate, dendrite tip growth, etc. *naturally* arise from the averaging procedure; this point may seem unimportant, but there has, in fact, been quite a controversy over the correct

form of some of the equations,[134] and some confusion over how to best incorporate, for example, columnar dendrite tip undercooling in macroscopic models.[135]

- The averaged conservation equations explicitly contain microscale parameters such as the phase volume fractions, grain density, interfacial area concentration, local diffusion lengths, drag coefficients, etc.
- Local 'closure problems'[136,137] can be derived for the fluctuating variables (i.e. the difference between the average and microscopic value of a variable), which can then be solved for a small representative domain with periodic boundary conditions. This approach has recently been used[91,138] to determine various effective transport properties (e.g. permeability, solute diffusion-dispersion tensor, effective thermal conductivity, mass exchange coefficients, etc.) for a columnar mushy zone.

The application of the multiphase/multiscale model of Wang and Beckermann to predict macrosegregation during dendritic alloy solidification, with simultaneous melt convection and grain movement, is illustrated in the following example.[130] An Al–4 wt-%Cu alloy solidifies in an equiaxed fashion inside a rectangular cavity cooled from the left sidewall. Figure 19 shows the predicted evolution of the grain density (i.e. the number of grains per unit volume). Free grains nucleate first near the cooled sidewall, and are swept into the central part of the cavity by the thermosolutal melt flow. Once the superheat is dissipated, the melt surrounding the free equiaxed grains becomes undercooled and the grains will grow. Later, when the grains have grown to a sufficient size, they settle and form a fixed bed of equiaxed crystals at the bottom of the cavity. This bed continues to grow in height as more free grains settle downward. The interface between the bed and the overlying region of undercooled melt, containing freely moving and growing grains, is characterised by a relatively sharp gradient in the grain density. The grain density in the bed itself is invariant. Upon complete solidification, a reduced grain density, and hence larger grains, can be observed in the upper part of the cavity; this can be attributed to the continuous sedimentation of grains out of this region. Because the local nucleation rate was set to a constant value, the grain density would have been uniform in the absence of grain movement. Therefore, all spatial variations in the grain density are directly due to grain movement.

The effects of grain movement, and of different nucleation rates, on macrosegregation are illustrated in Fig. 20. Figure 20*a* corresponds to a simulation where a stationary solid phase was assumed. Thermosolutal convection causes strong positive macrosegregation along the bottom wall and right sidewall of the cavity, because the cold, solute rich melt is heavy and flows downward during solidification. In addition, several (inverted) A segregates can be observed in the lower central region. Figure 20*b* shows the macrosegregation pattern for a simulation with moving grains, corresponding to the grain density plots of Fig. 19. Overall, the macrosegregation is less severe, and no channel segregates are predicted. This

Grain Density (m⁻³)   $10^8$   $5 \times 10^8$   $10^9$   $5 \times 10^9$
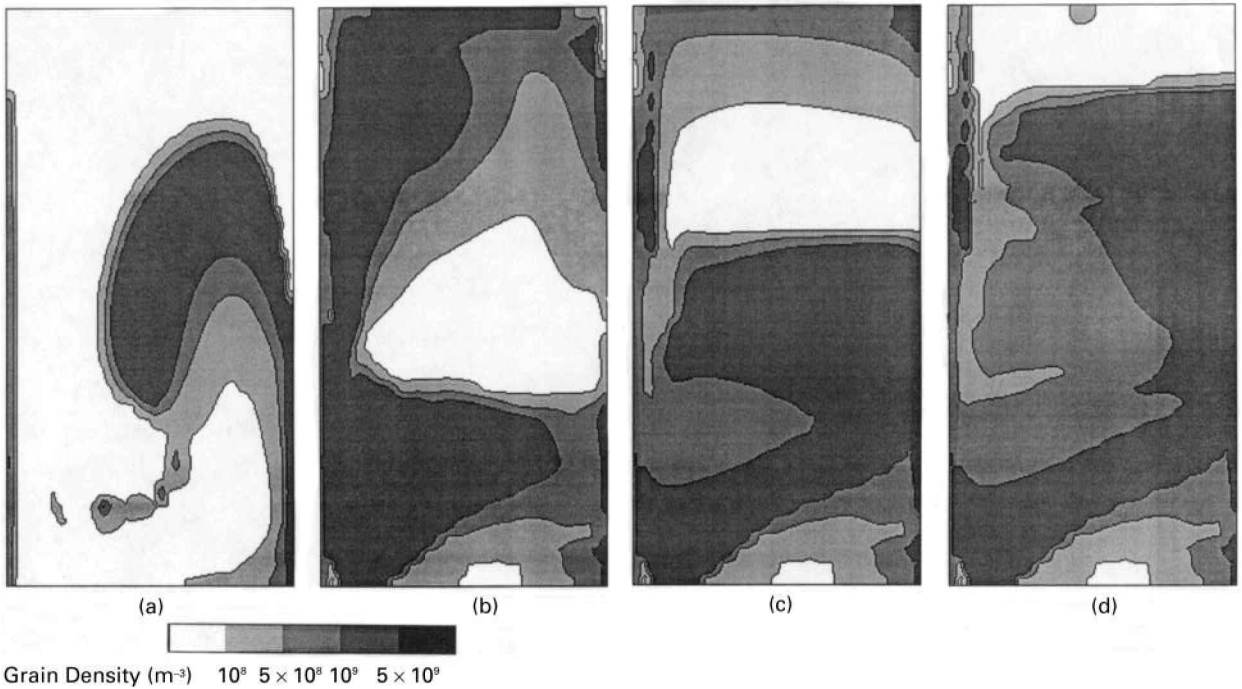
*a* 10 s; *b* 30 s; *c* 50 s; *d* 100 s

**19  Predicted evolution of grain density during equiaxed dendritic solidification of Al–4 wt-%Cu alloy with grain movement inside 5 × 10 cm rectangular cavity cooled from left sidewall**[130]



$C_{mix}$ (wt%)   2   4   6   8   10   12
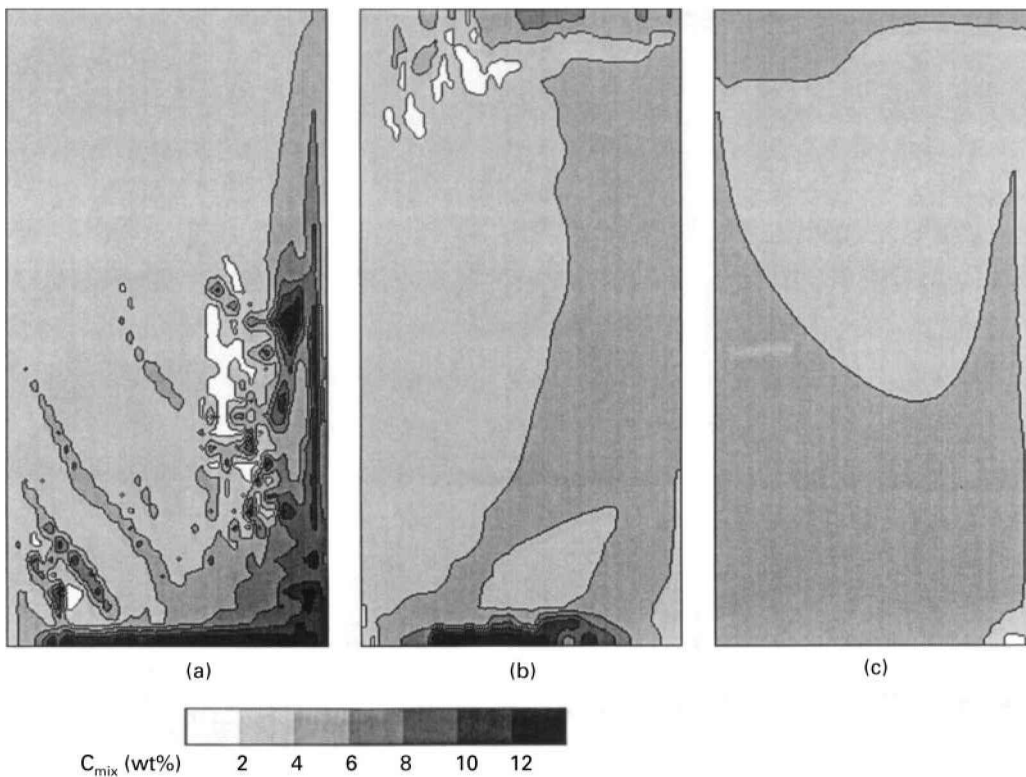
*a* stationary grains (low nucleation rate); *b* moving grains (low nucleation rate: corresponds to Fig. 19); *c* moving grains (high nucleation rate)

**20  Effect of grain movement and of different nucleation rates on predicted macrosegregation patterns in equiaxed dendritic solidification of Al–4 wt-%Cu alloy with grain movement inside 5 × 10 cm rectangular cavity cooled from left sidewall**[130]
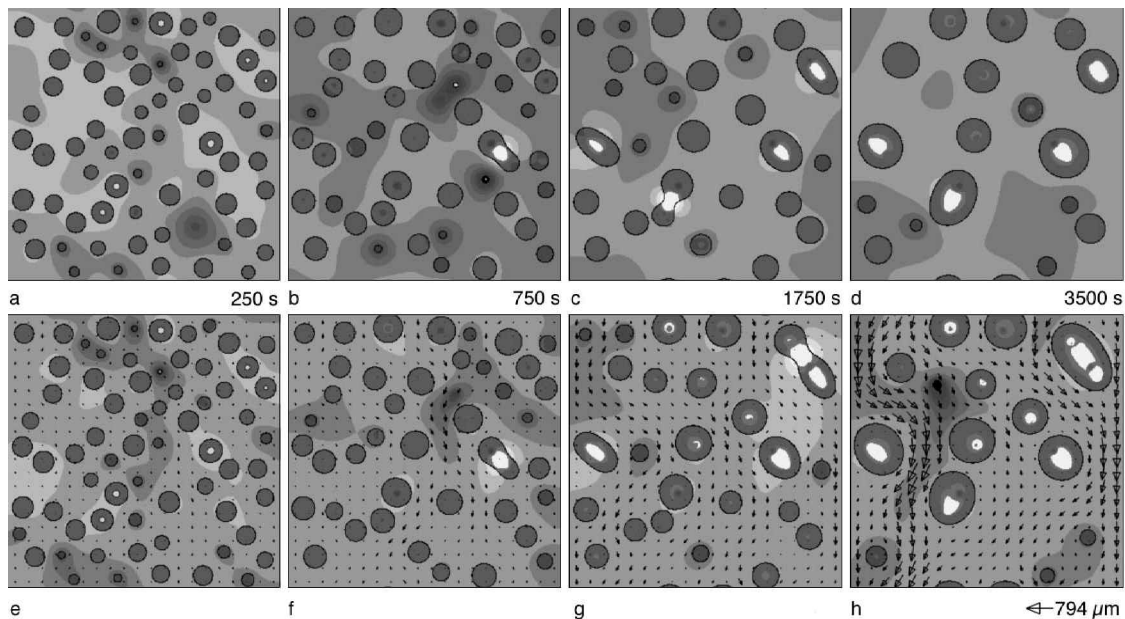
a–d simulation under purely diffusive conditions; e–h simulation with pressure drop of 0·2 N m$^{-2}$ applied in north–south direction (arrows are liquid velocity vectors)

**21   Phase field simulations of evolution of microstructure due to Ostwald ripening in Al–4 wt-%Cu alloy mush where solid fraction is constant at 0·207: domain is 0·81 mm square with periodic boundary conditions; black contour lines show solid/liquid interface; grey shades indicate Cu concentrations in liquid (10 equal intervals between 4·861 and 4·871 wt-%Cu) and solid (4 equal intervals between 0·682 and 0·6805 wt-%Cu)[147]**

can be attributed to the fact that both the solute rich liquid and the solute poor solid flow downward, resulting in less relative motion between the solid and liquid phases than in the case of a stationary solid. Even less macrosegregation is observed in Fig. 20c, where a higher nucleation rate was employed in the simulation. The higher nucleation rate results in smaller grains that closely follow the liquid motion until they pack. It should be noted that, in alloys where the solute rich liquid is lighter and the solid is more dense than the melt of the original composition, the settling of free grains causes negative macrosegregation at the bottom and positive macrosegregation at the top of the solidification domain. The classical macrosegregation pattern in a steel ingot (Fig. 3) is an example of that effect. However, in the Al–Cu system of Figs. 19 and 20, the solute rich melt is heavier, and the positive macrosegregation at the bottom of the cavity due to melt flow (Fig. 20a) is partially 'cancelled' by the settling of solute poor solid, resulting in less severe overall macrosegregation (Fig. 20b and c).

A comparison of the multiphase/multiscale model with experiments conducted using the transparent model alloy NH$_4$Cl–H$_2$O revealed good agreement between the measured and predicted flow patterns and crystal settling rates during solidification.[131] While the multiphase/multiscale model appears to provide a suitable framework for coupled micro-structure–macrosegregation modelling, many uncertainties still exist. For example, only approximate models are available for the effects of flow on grain generation (including fragmentation), dendrite tip growth, two phase rheology, etc. Concentrated research efforts are underway to clarify these and

other questions (*see* e.g. Refs. 121–124, 139), but much work remains. One important goal would be to predict macrosegregation in castings that feature a columnar to equiaxed transition.

## Direct numerical simulation

During the last decade, much progress has been made in the direct numerical simulation of solidification microstructure development. In particular, the phase field method has been used to predict various complex growth patterns from first principles.[140–142] Beckermann *et al.*[143] have recently extended the phase field method to include melt convection. This new capability will allow for the detailed investigation of the effects of flow on the structure of the mush, dendrite tip growth,[144–146] microsegregation, fragmentation, and other flow related issues that have hampered coupled microstructure–macrosegregation modelling in the past. This modelling work is of particular importance, because such investigations are difficult to perform experimentally owing to the small scale of the phenomena involved.

An example of a microstructure simulation that has a direct bearing on modelling of macrosegregation is the recent study by Diepers *et al.*[147] They used the phase field method to model the flow through, and ripening of, an adiabatic Al–4 wt-%Cu alloy mush volume element, such as that shown in Fig. 2. Representative two-dimensional simulation results, with and without flow, are shown in Fig. 21. Ripening (or coarsening) causes the solid/liquid interfacial area to decrease with time. This, in turn, results in an increase in the permeability. However, it is important to realise that the ripening dynamics are influenced

by convection. In other words, the microstructure of the mush governs the flow, but the flow also influences the evolution of the microstructure. The simulations of Diepers *et al*. verified that, in accordance with classical ripening theories, the interfacial area decreases with the cube root of time when there is no flow. In the presence of flow, on the other hand, the interfacial area decreases with the square root of time. Diepers *et al*. also measured the permeability of the mush volume element from the simulation results, and found that the permeability normalised by the square of the interfacial area per unit solid volume is constant in time. By performing simulations with different volume fractions of solid inside the element, they were able to correlate the permeability with the various microstructural parameters present. Direct numerical simulations of flows through a unit cell inside a mushy zone in order to determine permeabilities have also been reported in Refs. 88–91, 148. However, in those studies the microstructure was taken to be static, and concurrent coarsening or solidification was not modelled.

While knowledge of the permeability of an evolving microstructure is important for present macrosegregation models, the simulations of Diepers *et al*.[147] also point the way toward the future of macrosegregation modelling through numerical simulations on the microscopic scale. In this way, all the microscopic phenomena would be directly taken into account, and the results could be used to assess and improve models that are based on averaging (such as those reviewed in the previous two sections). Presently, such microscopic simulations of macrosegregation formation cannot be performed on the scale of an entire casting. However, with some evolution in computing power, they would be realistic for scales of the order of several millimetres (requiring of the order of $10^9$ to $10^{12}$ grid points in three dimensions).

# Conclusions and future research needs

Modelling of macrosegregation has experienced major advances since the pioneering work of Flemings and co-workers in the mid-1960s. While some successes have been reported in predicting measured macrosegregation patterns in industrially relevant casting processes, there are still numerous areas where further development is required. Based on the present review, the basic phenomena that should receive increased research attention can be summarised as follows:
- macrosegregation in multicomponent alloys, taking into account the formation of multiple phases
- macrosegregation in the presence of grain structure transitions (e.g. columnar to equiaxed)
- macrosegregation due to deformation of the solid or mush
- macrosegregation due to movement of solid
- micro-/macrosegregation in the presence of undercooled, convecting liquid.

The resolution of these issues will not only require even more complex models, but also careful validation using specially designed experiments.

Furthermore, the resolution of melt flow patterns in numerical solutions of macrosegregation models

has often been inadequate, and most simulations reported in the literature are restricted to two dimensions. With the availability of increased computing power and more efficient numerical techniques, greater efforts should be made to reduce numerical inaccuracies and to resolve the highly three-dimensional, transient, and sometimes turbulent flow patterns present in often complex shaped castings. Some of these issues are already being addressed by various research groups (Refs. 70–72, 149–155) as well as by developers of commercial casting simulation codes.

It has become clear that numerous macrosegregation phenomena cannot be predicted without detailed consideration of the evolving microstructure. Thus, in many cases, further progress in macrosegregation modelling can only be made if the microstructure and grain structure transitions are predicted as well. While research in the area of solidification microstructures has traditionally focused on the prediction of phases and growth patterns in a diffusive environment, macrosegregation modelling requires a quantitative understanding of the convective interactions on a microscopic scale. A few of the outstanding research issues are:
- nucleation in a convective environment
- fragmentation and transport of fragments originating in the mushy zone or at outer surfaces
- effects of flow on the growth rates of the dendrite tips, eutectic front, etc.
- effects of flow on the evolution of dendrite arm spacings and other microstructural length scales
- two phase rheology of a melt laden with equiaxed grains.

Future research on any of the above issues will increasingly rely on first principles, direct numerical simulations of solidification with flow on a microscopic scale using, for example, the phase field method. These advances in modelling are especially important in light of the difficulties in performing accurate experimental measurements on a microscopic scale. However, the use of such microscale simulations to predict macrosegregation on the scale of an entire casting will probably not be an option until at least the year 2050 (Refs. 156, 157).

# Acknowledgements

# References

1. C. BECKERMANN and C. Y. WANG: in 'Annual review of heat transfer VI', Vol. 6, (ed. C. L. Tien), 115–198; 1995, New York, Begell House.
2. P. J. PRESCOTT and F. P. INCROPERA: in 'Advances in heat transfer', (ed. D. Poulikakos), 231–338; 1996, San Diego, CA, Academic Press.
3. H. COMBEAU, B. APPOLAIRE, and G. LESOULT: in 'Modeling of casting, welding and advanced solidification processes VIII', (ed. B. G. Thomas and C. Beckermann), 245–256; 1998, Warrendale, PA, TMS.

4.  M. C. FLEMINGS: in 'Modeling of casting, welding and advanced solidification processes VIII', (ed. B. G. Thomas and C. Beckermann), 1–13; 1998, Warrendale, PA, TMS.
5.  M. C. FLEMINGS and G. E. NEREO: *Trans. AIME*, 1967, 239, 1449–1461.
6.  M. C. FLEMINGS, R. MEHRABIAN, and G. E. NEREO: *Trans. AIME*, 1968, 242, 41–49.
7.  M. C. FLEMINGS and G. E. NEREO: *Trans. AIME*, 1968, 242, 50–55.
8.  R. MEHRABIAN, M. KEANE, AND M. C. FLEMINGS: *Metall. Trans.*, 1970, 1, 1209–1220.
9.  T. S. PIWONKA AND M. C. FLEMINGS: *Trans. AIME*, 1966, 236, 1157–1165.
10. D. APELIAN, M. C. FLEMINGS, and R. MEHRABIAN: *Metall. Trans.*, 1974, 5, 2533–2537.
11. R. MEHRABIAN, M. A. KEANE, AND M. C. FLEMINGS: *Metall. Trans.*, 1970, 1, 3238–3241.
12. S. KOU, D. R. POIRIER, AND M. C. FLEMINGS: *Metall. Trans. B*, 1978, 9B, 711–719.
13. R. MEHRABIAN AND M. C. FLEMINGS: *Metall. Trans.*, 1970, 1, 455–464.
14. T. FUJII, D. R. POIRIER, AND M. C. FLEMINGS: *Metall. Trans. B*, 1979, 10B, 331–339.
15. S. D. RIDDER, S. KOU, and R. MEHRABIAN: *Metall. Trans. B*, 1981, 12B, 435–447.
16. V. C. PRANTIL and P. R. DAWSON: in HTD-Vol. 29, 47–54; 1983, New York, ASME.
17. R. N. HILLS, D. E. LOPER, and P. H. ROBERTS: *Q. J. Mech. Appl. Math.*, 1983, 36, 505–539.
18. D. A. DREW: *Ann. Rev. Fluid Mech.*, 1983, 15, 261–291.
19. W. D. BENNON and F. P. INCROPERA: *Int. J. Heat Mass Transf.*, 1987, 30, 2161–2170.
20. C. BECKERMANN and R. VISKANTA: *PhysicoChem. Hydrodyn.*, 1988, 10, 195–213.
21. V. R. VOLLER, A. D. BRENT, and C. PRAKASH: *Int. J. Heat Mass Transf.*, 1989, 32, 1718–1731.
22. S. GANESAN and D. R. POIRIER: *Metall. Trans. B*, 1990, 21B, 173–181.
23. D. R. POIRIER, P. J. NANDAPURKAR, and S. GANESAN: *Metall. Trans. B*, 1991, 22B, 889–900.
24. W. D. BENNON and F. P. INCROPERA: *Metall. Trans. B*, 1987, 18B, 611–616.
25. S. D. FELICELLI, J. C. HEINRICH, and D. R. POIRIER: *Metall. Trans. B*, 1991, 22B, 847–859.
26. C. BECKERMANN and R. VISKANTA: *Appl. Mech. Rev.*, 1993, 46, 1–27.
27. M. G. WORSTER: *Ann. Rev. Fluid Mech.*, 1997, 29, 91–122.
28. V. R. VOLLER: in 'Advances in numerical heat transfer', Vol. 1, (ed. W. J. Minkowycz and E. M. Sparrow), 341–375; 1996, Washington, DC, Taylor & Francis.
29. V. R. VOLLER, C. R. SWAMINATHAN, and B. G. THOMAS: *Int. J. Numer. Methods Eng.*, 1990, 30, 875–898.
30. C. PRAKASH and V. R. VOLLER: *Numer. Heat Transf. B*, 1989, 15, 171–189.
31. M. C. FLEMINGS: 'Solidification processing'; 1974, New York, McGraw-Hill.
32. J. P. GU and C. BECKERMANN: *Metall. Mater. Trans. A*, 1999, 30A, 1357–1366.
33. I. VANNIER, H. COMBEAU, and G. LESOULT: *Mater. Sci. Eng.*, 1993, A173, 317–321.
34. M. C. SCHNEIDER and C. BECKERMANN: *Metall. Mater. Trans. A*, 1995, 26A, 2373–2388.
35. S. SUNDARRAJ and G. A. MILLER: Proc. Merton C. Flemings Symp. on 'Solidification and materials processing', (ed. R. Abbaschian *et al.*), 311–316; 2001, Warrendale, PA, TMS.
36. A. OLSSON, R. WEST, and H. FREDRIKSSON: *Scand. J. Metall.*, 1986, 15, 104–112.
37. M. C. FLEMINGS: *ISIJ Int.*, 2000, 40, 833–841.
38. T. KAJITANI, J.-M. DREZET, and M. RAPPAZ: *Metall. Mater. Trans. A*, 2001, 32A, 1479–1491.
39. G. LESOULT and S. SELLA: *Solid State Phenom.*, 1988, 3–4, 167–178.
40. H. FREDRIKSSON: *Can. Metall. Q.*, 1991, 30, 235–244.
41. M. R. ABOUTALEBI, M. HASAN, and R. I. L. GUTHRIE: *Metall. Mater. Trans. B*, 1995, 26B, 731–744.
42. H. L. YANG, L. G. ZHAO, X. Z. ZHANG, K. W. DENG, W. C. LI, and Y. GAN: *Metall. Mater. Trans. B*, 1998, 29B, 1345–1356.
43. S. Y. LEE, S. I. CHUNG, and C. P. HONG: in 'Modeling of casting, welding and advanced solidification processes IX', (ed. P. R. Sahm *et al.*), 648–655; 2000, Aachen, Shaker Verlag.

44. C. M. OLDENBURG and F. J. SPERA: *Numer. Heat Transf. B*, 1992, 21, 217–229.
45. S. K. CHOUDHARY and A. GOSH: *ISIJ Int.*, 1994, 34, 338–345.
46. C. M. RAIHLE and H. FREDRIKSSON: *Metall. Mater. Trans. B*, 1994, 25B, 123–133.
47. M. EL-BEALY and H. FREDRIKSSON: *Scand. J. Metall.*, 1994, 23, 140–150.
48. M. EL-BEALY: *Scand. J. Metall.*, 1995, 24, 106–120.
49. R. J. A. JANSSEN, G. C. J. BART, M. C. M. CORNELISSEN, and J. M. RABENBERG: *Appl. Sci. Res.*, 1994, 52, 21–35.
50. K. MIYAZAWA and K. SCHWERDTFEGER: *Arch. Eisenhüttenwes.*, 1981, 52, 415–422.
51. I. OHNAKA and T. SHIMAZU: Proc. 6th Int. Iron and Steel Congress, Nagoya, Japan, 1990, 681–688; 1990, Tokyo, Iron and Steel Institute of Japan.
52. T. L. FINN, M. G. CHU, and W. D. BENNON: in 'Micro/macro scale phenomena in solidification', (ed. C. Beckermann *et al.*), 17–26; 1992, New York, ASME.
53. A. V. REDDY and C. BECKERMANN: *Metall. Mater. Trans. B*, 1997, 28B, 479–489.
54. A. MO: *Int. J. Heat Mass Transf.*, 1993, 36, 4335–4340.
55. E. HAUG, A. MO, and H. J. THEVIK: *Int. J. Heat Mass Transf.*, 1995, 38, 1553–1563.
56. H. J. THEVIK and A. MO: *Int. J. Heat Mass Transf.*, 1997, 40, 2055–2065.
57. H. J. THEVIK and A. MO: *Metall. Mater. Trans. B*, 1997, 28B, 665–669.
58. H. J. THEVIK, A. MO, and T. RUSTEN: *Metall. Mater. Trans. B*, 1999, 30B, 135–142.
59. M. G. CHU and J. E. JACOBY: in 'Light metals 1990', (ed. C. M. Bickert), 925–930; 1990, Warrendale, PA, TMS.
60. A. V. REDDY and C. BECKERMANN: in 'Materials processing in the computer age II', (ed. V. R. Voller *et al.*), 89–102; 1995, Warrendale, PA, TMS.
61. C. J. VREEMAN, M. J. M. KRANE, and F. P. INCROPERA: *Int. J. Heat Mass Transf.*, 2000, 43, 677–686.
62. C. J. VREEMAN and F. P. INCROPERA: *Int. J. Heat Mass Transf.*, 2000, 43, 687–704.
63. A. MO and H. J. THEVIK: *Metall. Mater. Trans. A*, 1998, 29A, 2189–2194.
64. A. JOLY, G. U. GRUN, D. DALOZ, H. COMBEAU, and G. LESOULT: *Mater. Sci. Forum*, 2000, 329, 111–119.
65. M. C. SCHNEIDER, J. P. GU, C. BECKERMANN, W. J. BOETTINGER, and U. R. KATTNER: *Metall. Mater. Trans. A*, 1997, 28A, 1517–1531.
66. J. P. GU, C. BECKERMANN, and A. F. GIAMEI: *Metall. Mater. Trans. A*, 1997, 28A, 1533–1542.
67. S. D. FELICELLI, D. R. POIRIER, and J. C. HEINRICH: *J. Cryst. Growth*, 1997, 177, 145–161.
68. S. D. FELICELLI, D. R. POIRIER, A. F. GIAMEI, and J. C. HEINRICH: *JOM*, 1997, 49, (3), 21–25.
69. S. D. FELICELLI, J. C. HEINRICH, and D. R. POIRIER: *Int. J. Numer. Methods Fluids*, 1998, 27, 207–227.
70. D. G. NEILSON and F. P. INCROPERA: *Numer. Heat Transf. A*, 1993, 23, 1–20.
71. S. D. FELICELLI, J. C. HEINRICH, and D. R. POIRIER: *J. Cryst. Growth*, 1998, 191, 879–888.
72. S. D. FELICELLI, D. R. POIRIER, and J. C. HEINRICH: *Metall. Mater. Trans. B*, 1998, 29B, 847–855.
73. C. BECKERMANN, J. P. GU, and W. J. BOETTINGER: *Metall. Mater. Trans. A*, 2000, 31A, 2545–2557.
74. T. M. POLLOCK and W. H. MURPHY: *Metall. Mater. Trans. A*, 1996, 27A, 1081–1094.
75. P. AUBURTIN, T. WANG, S. L. COCKCROFT, and A. MITCHELL: *Metall. Mater. Trans. A*, 2000, 31A, 801–811.
76. A. MORTENSEN and V. J. MICHAUD: *Metall. Trans. A*, 1990, 21A, 2059–2072.
77. V. J. MICHAUD and A. MORTENSEN: *Metall. Trans. A*, 1992, 23A, 2263–2280.
78. P. JARRY, V. J. MICHAUD, A. MORTENSEN, A. DUBUS, and R. TIRARD-COLLET: *Metall. Trans. A*, 1992, 23A, 2281–2289.
79. A. MORTENSEN and I. JIN: *Int. Mater. Rev.*, 1992, 37, 101–128.
80. R. J. FELLER and C. BECKERMANN: *Metall. Mater. Trans. B*, 1997, 28B, 1165–1183.
81. Q. HAN and J. D. HUNT: *ISIJ Int.*, 1995, 35, 693–699.
82. J. GIULIANI and K. VAFAI: *J. Fluid. Eng.*, 1999, 121, 155–162.
83. J. A. SEKHAR and R. TRIVEDI: in 'Solidification of metal matrix composites', (ed. P. Rohatgi), 39–50; 1990, Warrendale, PA, TMS.

84. H. K. MOON, J. A. CORNIE, AND M. C. FLEMINGS: *Mater. Sci. Eng.*, 1991, A144, 253–265.
85. M. C. SCHNEIDER, C. BECKERMANN, D. M. LIPINSKI, and W. SCHAEFER: in 'Modeling of casting, welding and advanced solidification processes VIII', (ed. B. G. Thomas and C. Beckermann), 257–264; 1998, Warrendale, PA, TMS.
86. D. R. POIRIER: *Metall. Trans. B*, 1987, 18B, 245–255.
87. S. GANESAN, C. L. CHAN, and D. R. POIRIER: *Mater. Sci. Eng.*, 1992, A151, 97–105.
88. M. S. BHAT, D. R. POIRIER, J. C. HEINRICH, and D. NAGELHOUT: *Scr. Metall. Mater.*, 1994, 31, 339–344.
89. M. S. BHAT, D. R. POIRIER, and J. C. HEINRICH: *Metall. Mater. Trans. B*, 1995, 26B, 1091–1092.
90. M. S. BHAT, D. R. POIRIER, and J. C. HEINRICH: *Metall. Mater. Trans. B*, 1995, 26B, 1049–1056.
91. B. GOYEAU, T. BENIHADDADENE, D. GOBIN, and M. QUINTARD: *Metall. Mater. Trans. B*, 1999, 30B, 613–622.
92. C. Y. WANG, S. AHUJA, C. BECKERMANN, and H. C. DE GROH III: *Metall. Trans. B*, 1995, 26B, 111–119.
93. O. NIELSEN, L. ARNBERG, A. MO, and H. THEVIK: *Metall. Mater. Trans. A*, 1999, 30A, 2455–2462.
94. O. NIELSEN and L. ARNBERG: *Metall. Mater. Trans. A*, 2000, 31A, 3149–3153.
95. D. R. POIRIER and S. GANESAN: *Mater. Sci. Eng.*, 1992, A157, 113–123.
96. P. OCANSEY and D. R. POIRIER: *Mater. Sci. Eng.*, 1993, A171, 231–240.
97. A. J. DUNCAN, Q. HAN, and S. VISWANATHAN: *Metall. Mater. Trans. A*, 1999, 30A, 745–750.
98. H. C. DE GROH III, P. D. WEIDMAN, D. ZAKHEM, S. AHUJA, and C. BECKERMANN: *Metall. Trans. B*, 1993, 24B, 749–753.
99. L. ARNBERG, G. CHAI, and L. BACKERUD: *Mater. Sci. Eng.*, 1993, A173, 101–103.
100. M. RAPPAZ and V. R. VOLLER: *Metall. Mater. Trans. A*, 1990, 21A, 749–753.
101. S. SUNDARRAJ and V. R. VOLLER: *Int. Commun. Heat Mass Transf.*, 1993, 21, 189–198.
102. S. SUNDARRAJ and V. R. VOLLER: *Int. J. Numer. Methods Heat Fluid Flow*, 1997, 7, 181–199.
103. A. MO: *Metall. Trans. B*, 1994, 25B, 597–605.
104. H. COMBEAU, J.-M. DREZET, A. MO, and M. RAPPAZ: *Metall. Mater. Trans. A*, 1996, 27A, 2305–2313.
105. M. C. SCHNEIDER and C. BECKERMANN: *Int. J. Heat Mass Transf.*, 1995, 38, 3455–3473.
106. H. COMBEAU and A. MO: *Metall. Mater. Trans. A*, 1997, 28A, 2705–2714.
107. C. BECKERMANN AND M. C. SCHNEIDER: *ISIJ Int.*, 1995, 35, 1300–1307.
108. M. J. M. KRANE and F. P. INCROPERA: *Int. J. Heat Mass Transf.*, 1997, 40, 3827–3835.
109. M. J. M. KRANE and F. P. INCROPERA: *Int. J. Heat Mass Transf.*, 1997, 40, 3837–3847.
110. M. J. M. KRANE, F. P. INCROPERA, and D. R. GASKELL: *Metall. Mater. Trans. A*, 1998, 29A, 843–853.
111. M. EL-BEALY and H. FREDRIKSSON: *Metall. Mater. Trans. B*, 1996, 27B, 999–1014.
112. M. M'HAMDI, M. BOBADILLA, H. COMBEAU, and G. LESOULT: in 'Modeling of casting, welding and advanced solidification processes VIII', (ed. B. G. Thomas and C. Beckermann), 375–382; 1998, Warrendale, PA, TMS..
113. M. M'HAMDI, H. COMBEAU, and G. LESOULT: *Int. J. Numer. Methods Heat Fluid Flow*, 1999, 9, 296–317.
114. C. Y. WANG and C. BECKERMANN: *Int. J. Multiphase Flow*, 1993, 19, 397–407.
115. C. Y. WANG and C. BECKERMANN: *Metall. Trans. A*, 1993, 24A, 2787–2802.
116. C. Y. WANG and C. BECKERMANN: *Mater. Sci. Eng.*, 1993, A171, 199–211.
117. C. Y. WANG and C. BECKERMANN: *Metall. Trans. A*, 1994, 25A, 1081–1093.
118. I. DUSTIN and W. KURZ: *Z. Metallkd.*, 1986, 77, 265–273.
119. M. RAPPAZ AND PH. THEVOZ: *Acta Metall.*, 1987, 35, 1487–1497.
120. X. TONG and C. BECKERMANN: *J. Cryst. Growth*, 1998, 187, 289–302.
121. A. RAMANI and C. BECKERMANN: *Scr. Mater.*, 1997, 36, 633–638.
122. B. APPOLAIRE, V. ALBERT, H. COMBEAU, and G. LESOULT: *Acta Mater.*, 1998, 46, 5851–5862.
123. B. APPOLAIRE, V. ALBERT, H. COMBEAU, and G. LESOULT: *ISIJ Int.*, 1999, 39, 263–270.
124. S. GERARDIN, H. COMBEAU, and G. LESOULT: *J. Phys. IV*, 2001, 11, 143–150.
125. M. RAPPAZ: *Int. Mater. Rev.*, 1989, 34, 93–123.
126. CH.-A. GANDIN, T. JALANTI, and M. RAPPAZ: in 'Modeling of casting, welding and advanced solidification processes VIII', (ed. B. G. Thomas and C. Beckermann), 363–374; 1998, Warrendale, PA, TMS.
127. M. RAPPAZ, J. L. DESBIOLLES, and C. A. GANDIN: *Mater. Sci. Forum*, 2000, 329, 389–396.
128. J. NI and C. BECKERMANN: *Metall. Trans. B*, 1991, 22B, 349–361.
129. C. Y. WANG and C. BECKERMANN: *Metall. Mater. Trans. A*, 1996, 27A, 2754–2764.
130. C. Y. WANG and C. BECKERMANN: *Metall. Mater. Trans. A*, 1996, 27A, 2765–2783.
131. C. BECKERMANN and C. Y. WANG: *Metall. Mater. Trans. A*, 1996, 27A, 2784–2795.
132. J. NI and F. P. INCROPERA: *Int. J. Heat Mass Transf.*, 1995, 38, 1271–1284.
133. J. NI and F. P. INCROPERA: *Int. J. Heat Mass Transf.*, 1995, 38, 1285–1296.
134. P. J. PRESCOTT, F. P. INCROPERA, and W. D. BENNON: *Int. J. Heat Mass Transf.*, 1991, 34, 2351–2359.
135. S. C. FLOOD and J. D. HUNT: *Appl. Sci. Res.*, 1987, 44, 27–42.
136. J. BARRERE, O. GIPOULOUX, and S. WHITAKER: *Transp. Porous Media*, 1992, 7, 209–222.
137. M. QUINTARD and S. WHITAKER: *Transp. Porous Media*, 1994, 15, 31–49.
138. P. BOUSQUET-MELOU, B. GOYEAU, M. QUINTARD, F. FICHOT, and D. GOBIN: in 'Modeling of casting, welding and advanced solidification processes IX', (ed. P. R. Sahm *et al*.), 616–623; 2000, Aachen, Shaker Verlag.
139. C. J. PARADIES, G. T. KIM, M. E. GLICKSMAN, and R. N. SMITH: in 'Modeling of casting, welding and advanced solidification processes VI', (ed. T. S. Piwonka *et al*.), 309–316; 1993, Warrendale, PA, TMS.
140. A. A. WHEELER, W. J. BOETTINGER, and G. B. MCFADDEN: *Phys. Rev. A*, 1992, 45, 7424.
141. R. KOBAYASHI: *Physica D*, 1993, 63, 410.
142. A. KARMA and W. J. RAPPEL: *Phys. Rev. E*, 1998, 57, 4323.
143. C. BECKERMANN, H. J. DIEPERS, I. STEINBACH, A. KARMA, and X. TONG: *J. Comput. Phys.*, 1999, 154, 468–496.
144. X. TONG, C. BECKERMANN, and A. KARMA: *Phys. Rev. E*, 2000, 61, R49–R52.
145. X. TONG, C. BECKERMANN, A. KARMA, and Q. LI: *Phys. Rev. E*, 2001, 63, 061601.
146. J. H. JEONG, N. GOLDENFELD, and J. A. DANTZIG: *Phys. Rev. E*, 2001, 64, 041602.
147. H. J. DIEPERS, C. BECKERMANN, and I. STEINBACH: *Acta Mater.*, 1999, 47, 3663–3678.
148. J. F. MCCARTHY: *Acta Metall. Mater.*, 1994, 42, 1573–1581.
149. P. J. PRESCOTT and F. P. INCROPERA: *J. Heat Transf.*, 1995, 117, 716–724.
150. H.-W. HUANG, J. C. HEINRICH, and D. R. POIRIER: *Numer. Heat Transf. A*, 1996, 29, 639–644.
151. P. K. SUNG, D. R. POIRIER, and S. D. FELICELLI: *Int. J. Numer. Methods Fluids*, 2001, 35, 357–370.
152. C. FRUEH, D. R. POIRIER, and S. D. FELICELLI: *Metall. Mater. Trans. A*, 2000, 31A, 3129–3135.
153. P. K. SUNG, D. R. POIRIER, and S. D. FELICELLI: *Metall. Mater. Trans. A*, 2001, 32A, 202–207.
154. N. AHMAD, H. COMBEAU, J. L. DESBIOLLES, T. JALANTI, G. LESOULT, J. RAPPAZ, M. RAPPAZ, and C. STOMP: *Metall. Mat. Trans. A*, 1998, 29A, 617–630.
155. TH. U. KAEMPFER and M. RAPPAZ: in 'Modeling of casting, welding and advanced solidification processes IX', (ed. P. R. Sahm *et al*.), 640–647; 2000, Aachen, Shaker Verlag.
156. V. R. VOLLER: Proc. 2001 TMS Fall Extraction and Process Metallurgy Meeting: 'Computational modeling of materials, minerals, and metals', (ed. M. Cross), 41–61; 2001, Warrendale, PA, TMS (in press).
157. V. R. VOLLER and F. PORTE-AGEL: *J. Comput. Phys.*, 2002, 179, 698–703.